

## Absolute Winding Number Differentiates Spatial Navigation Strategies with Genetic Risk for Alzheimer's Disease

1        **Alexandra Badea<sup>1,2,3,4\*#</sup>, Didong Li<sup>5,6#</sup>, Andrei R Niculescu<sup>1</sup>, Robert J Anderson<sup>1</sup>, Jacques A**  
2        **Stout<sup>3</sup>, Christina L Williams<sup>7</sup>, Carol A Colton<sup>2</sup>, Nobuyo Maeda<sup>8</sup>, David B Dunson<sup>9</sup>**

3        <sup>1</sup>Department of Radiology, Duke University, Durham, NC, USA

4        <sup>2</sup>Department of Neurology, Duke University, Durham, NC, USA

5        <sup>3</sup> Brain Imaging and Analysis Center, Duke University, Durham, NC, USA

6        <sup>4</sup> Biomedical Engineering, Duke University, Durham, NC

7        <sup>5</sup> Department of Computer Science, Princeton University, Princeton, NJ

8        <sup>6</sup> Department of Biostatistics, UCLA, Los Angeles, CA

9        <sup>7</sup> Department of Psychology and Neuroscience, Duke University, Durham, NC, USA

10        <sup>8</sup>Department of Pathology and Laboratory Medicine, UNC, Chapel Hill, NC

11        <sup>9</sup> Department of Statistical Science, Duke University, Durham, NC

12        **\* Correspondence:**

13        Alexandra Badea, PhD

14        [alexandra.badea@duke.edu](mailto:alexandra.badea@duke.edu)

15        **#These authors have contributed equally, and share first authorship**

16        **Keywords: APOE, Alzheimer's disease, brain, mouse, connectivity, memory, MRI**

17

18

19 **Abstract**

20 Spatial navigation and orientation are emerging as promising markers for altered cognition in  
21 prodromal Alzheimer's disease, and even in cognitively normal individuals at risk for Alzheimer's  
22 disease. The different APOE gene alleles confer various degrees of risk. The APOE2 allele is  
23 considered protective, APOE3 is seen as control, while APOE4 carriage is the major known genetic  
24 risk for Alzheimer's disease. We have used mouse models carrying the three humanized APOE alleles  
25 and tested them in a spatial memory task in the Morris water maze. We introduce a new metric, the  
26 absolute winding number, to characterize the spatial search strategy, through the shape of the swim  
27 path. We show that this metric is robust to noise, and works for small group samples. Moreover, the  
28 absolute winding number better differentiated APOE3 carriers, through their straighter swim paths  
29 relative to both APOE2 and APOE4 genotypes. Finally, this novel metric was sensitive to sex  
30 differences, supporting increased vulnerability in females. We hypothesized differences in spatial  
31 memory and navigation strategies are linked to differences in brain networks, and showed that different  
32 genotypes have different reliance on the hippocampal and caudate putamen circuits, pointing to a role  
33 for white matter connections. Moreover, differences were most pronounced in females. This departure  
34 from a hippocampal centric to a brain network approach may open avenues for identifying regions  
35 linked to increased risk for Alzheimer's disease, before overt disease manifestation. Further exploration  
36 of novel biomarkers based on spatial navigation strategies may enlarge the windows of opportunity for  
37 interventions. The proposed framework will be significant in dissecting vulnerable circuits associated  
38 with cognitive changes in prodromal Alzheimer's disease.

39

40 **1 Introduction**

41 Alzheimer's disease (AD) directly affected 6 millions Americans in 2021, and these numbers include  
42 more than 12% of women, and 9% of men older than 65 (Alzheimer's Association 2021). The disease  
43 starts before overt memory loss and difficulty thinking, but escapes detection for decades, by which  
44 time it is too late for current treatments to be effective. A strategy to overcome these limitations and to  
45 quicken the pace of discovery, is to study people at risk for AD. The largest known genetic risk factor  
46 for AD is linked to the APOE gene. Having one copy of the APOE4 allele can increase risk for late  
47 onset AD by 2 to 3 times while two copies can increase the risk by 12 times (Michaelson 2014). In  
48 contrast, the APOE2 allele is thought to decrease risk for AD, relative to control APOE3 carriers and  
49 at risk APOE4 carriers (Wu and Zhao 2016). Humanized mouse models expressing these three major  
50 human APOE isoforms (targeted replacement) (Sullivan et al. 1998) (Knouff et al. 2004) can also be  
51 used to model genetic risk for late onset Alzheimer's disease.

52 Studying human populations and animal models of genetic risk for AD gives us the possibility to identify  
53 early biomarkers of AD. While the main complaints in AD are memory impairment and difficulty thinking,  
54 these are detected late in the disease process. Spatial navigation and orientation symptomatology  
55 have also been reported in AD, while the method chosen and performance in spatial strategies may  
56 provide protection against hippocampal degeneration during aging (Bohbot et al. 2007a). It has been  
57 suggested that spatial navigation impairment, in particular for allocentric and real space configurations,  
58 occurs early in the development of AD and can be used for monitoring disease progression or for  
59 evaluation of presymptomatic AD (Hort et al. 2007). Recent studies suggest that midlife APOE4  
60 carriers exhibit changes in navigation patterns before any detectable symptom onset (Coughlan et al.  
61 2018).

62 While we know that the hippocampus plays an important role in spatial navigation, it is becoming  
63 increasingly clear that it does not act alone to determine the goal-directed navigation strategy, but in  
64 connection with circuits involving e.g. the subiculum, thalamus, cingulate cortex, fornix, hypothalamus  
65 (Bermudez-Contreras, Clark, and Wilber 2020), and the dorsal striatum. The caudate putamen circuitry  
66 is thought to convey contextual information and to help form place-reward associations (Stoianov et  
67 al. 2018), (Pennartz et al. 2011). This new information demands a shift from hippocampal centric  
68 approaches to more extended brain subnetworks. Elements of these networks may reveal differences  
69 in individuals at risk for AD, at prodromal stages, and thus provide new biomarkers.

70 One way to test such target circuits is through lesion studies, and those have revealed that the (dorsal)  
71 hippocampus, fornix (Eichenbaum, Stewart, and Morris 1990), striatum, basal forebrain, cerebellum  
72 and cerebral cortex lead to lower performance; and so does disconnecting regions relevant for spatial  
73 learning. Still, it is not fully understood how different anatomical network nodes are involved in the  
74 acquisition and maintenance of different types of information required for spatial navigation, and what  
75 are the relationships with the genotypes that confer risk for AD. For example, approximately 50% of  
76 young adults prefer to use a spatial strategy, while the other 50% prefer a response strategy (Iaria et  
77 al. 2003). The spatial strategy involves using relationships between landmarks, and is thought to  
78 depend on the hippocampus (Bohbot, Iaria, and Petrides 2004). The response strategy involves  
79 learning stimulus-response associations, such as a series of right and left turns from specific points in  
80 space (McDonald and White 1994), and is thought to depend on the caudate putamen. The literature  
81 supports that the dorsal striatum is involved in stimulus-response learning, while the hippocampus  
82 mediates place learning. Moreover, increased gray matter density in the caudate nucleus has been  
83 associated with less gray matter in the hippocampus and vice versa. Therefore, navigation strategies  
84 are sensitive to the predominant use of gray matter in the hippocampus and caudate (Konishi et al.  
85 2016) memory systems. Such relationships have been shown for the gray matter (Bohbot et al. 2007b)  
86 in humans, but the role of white matter tracts in modulating performance in spatial navigation has been

87 less explored, in particular in relation to APOE genotypes. There is a need to better understand the  
88 role of different brain networks comprised of gray matter nuclei and their white matter connections, and  
89 how they confer vulnerability to AD. The differential roles between the two memory systems relying on  
90 the hippocampus and caudate putamen, and their associated brain circuits can be characterized using  
91 fMRI or diffusion weighted MRI and tractography, and may have the potential to reveal new and early  
92 markers in APOE carriers with different genetic risk levels.

93 Current studies have not consistently shown hippocampal atrophy in APOE4 carriers, in the absence  
94 of overt AD pathology. Some studies reported decreased hippocampal volume in young and old  
95 cognitively normal APOE4 carriers (Crivello et al., 2010; O'Dwyer et al., 2012; Wishart et al., 2006),  
96 while other did not find hippocampal atrophy (Haller et al., 2017; Honea et al., 2009). The structural  
97 covariance of different brain regions in relation to cognitive changes in prodromal AD has been less  
98 studied, but also points to more extended networks, where structural covariance patterns indicate  
99 differences with genotype (Novellino et al. 2019). Inverse correlation between hippocampus and  
100 caudate putamen and between these regions' gray matter and the preference for a spatial strategy  
101 has been shown (Bohbot et al. 2007b), but how these relationships are altered in relation to APOE is  
102 less known. This supports a need to investigate other regions beyond the hippocampus to understand  
103 the vulnerability of APOE4 carriers to AD (Crivello et al., 2010). It remains to be seen if extended brain  
104 circuits involved in spatial navigation may offer novel targets.

105 To assess spatial navigation strategies in subjects at risk is noninvasive and inexpensive. These  
106 assessments can complement more invasive molecular and mechanistic studies in animal models.  
107 The Morris Water Maze (MWM) is a popular tool to test spatial learning and memory, and navigation  
108 strategies, and was originally designed for animal tests. MWM like tests have also been designed and  
109 extended to humans, e.g. using virtual reality (Hodgetts et al. 2020). In the MWM test (Morris et al.  
110 1982) mice are placed in a circular pool and required to swim to a hidden platform beneath the surface  
111 using cues. MWM has long been thought as a test of hippocampal function, but more recently  
112 performance has been linked to the coordinated action of regions constituting a network (Hodgetts et  
113 al. 2020). Most often the performance in the water maze is described by the escape latency, or distance  
114 swam until the animals find the hidden platform. Search strategies are less often described, and rarely  
115 quantified, e.g. as manually scored percentage of time/distance spent using different strategies such  
116 as spatial, systematic, or looping search patterns. Using such techniques has helped identify increased  
117 chaining/loopiness following parietal cortex injuries (Brody and Holtzman 2006; Tucker, Velosky, and  
118 McCabe 2018) (Brabazon et al. 2017). In this paper we introduce a novel metric to characterize the  
119 search strategy, or loopiness of the swim path, the absolute winding number, and we assess its ability  
120 to discriminate between carriers of the three major APOE alleles.

121 Finally, we related changes in swim path shape, or search strategy, to imaging metrics derived from  
122 high resolution, high field MRI. For our analyses we selected two regions involved in spatial navigation,  
123 the hippocampus and the caudate putamen, as well as their major connections, through fimbria and  
124 fornix on one hand, and the internal capsule on the other. We added the cerebellar white matter to  
125 examine its role in modulating the search strategy as well, although this region is frequently used as a  
126 control region in AD studies. More recently the cerebellum has emerged as also having a role in  
127 learning, and it has been suggested it may interact with the hippocampus (Babayan et al. 2017),  
128 perhaps via other regions, including the retrosplenial cortex (Rochefort, Lefort, and Rondi-Reig 2013).

129 Our goals were to dissect whether spatial learning and memory circuits are differentially modulated by  
130 APOE isoforms, in the absence of AD pathology, and whether female sex confers increased  
131 vulnerability. Animal behavior was assessed in the Morris water maze in mouse models that express  
132 either human APOE2, APOE3, or APOE4 alleles, to reveal the impact of APOE genotype on brain  
133 circuit vulnerability in aging/AD. In a subset of mice, we have compared how learning and memory  
134 markers relate to the hippocampus and striatum structural phenotypes, using diffusion weighted

135 imaging to characterize morphometry through volume changes between genotypes, microstructural  
136 properties through fractional anisotropy, and connectivity through degree and clustering coefficient.

137 Our outcomes include factors such as behavior characteristics of spatial learning and memory,  
138 morphometry and texture based on MR imaging markers, and tractography based connectomics. We  
139 introduced a novel marker to the traditional distance measures, to characterize the complexity of the  
140 navigation strategy in the MWM, through an absolute winding number. This describes the loopiness of  
141 the swim path of mice tasked to locate a submerged platform in the Morris Water Maze, in a quantitative  
142 manner that makes it amenable to compare such strategies directly, and adds to the existing battery  
143 of MWM based metrics. We compared these behavioral and imaging markers with genotype, and sex.  
144 We build models to help distinguish how navigation strategies map to different brain regions and  
145 circuits in mice with the three major APOE alleles. Our analyses revealed that both genotype and  
146 female sex play a role, differentiating the three APOE alleles, and that the absolute winding number  
147 adds a robust and sensitive marker that may find translational applications if added to human studies  
148 evaluating genetic risk for AD.

149

150 **2 Methods**

151 **2.1 Animals**

152 To dissect how brain circuits vulnerable in aging and AD are modulated by the three major APOE  
153 isoforms, we have examined spatial learning and memory function using the Morris Water Maze test,  
154 in relation to morphometric and connectivity characteristics of the hippocampal, striatal and cerebellar  
155 circuits, as determined from diffusion weighted based MRI.

156 We used 12 month old humanized mice modeling genetic risk for late onset Alzheimer's disease  
157 expressing the three major human APOE alleles (targeted replacement). Mice were homozygous for  
158 the APOE2 allele, thought to be protective against Alzheimer's disease; APOE3, thought as the control  
159 gene variant, or APOE4, which is the major known genetic risk for late onset AD. Animals included  
160 both male and female sexes (**Table 1**).

161

Genotype	No Animals	Males	Female	Mean Age (months)	SD Age (months)
APOE2	13	8	5	12.64	0.70
APOE3	17	6	11	12.70	0.98
APOE4	24	13	11	12.47	1.43

162 **Table1. Animal groups distribution by genotype, sex, and age range.**

163

164 **2.2 Spatial Learning and Memory Testing**

165 Mice were handled for 5 days prior to behavioral testing to habituate to the researchers performing the  
166 tests, and to water. Spatial learning and memory were assessed using the Morris Water maze  
167 paradigm, similar to (Badea et al. 2019). The MWM tests a mouse's spatial memory and learning based  
168 on their preference for standing on solid ground, as opposed to swimming. Mice were trained for 5  
169 days in a circular swimming pool, filled with water rendered opaque using nontoxic white paint. The  
170 pool has 150 cm diameter, and behavior in the pool was tracked with a ceiling-mounted video camera,  
171 and the ANY-maze (Stoelting, Wood Dale, IL, United States) software. Four trials were administered

172 each day, in blocks of 2, separated by 30 minutes, and trials ended after 1 min maximum. Each trial  
173 consisted of placing the mouse into the water at one of four different starting positions, one in each  
174 quadrant. The quadrant order was varied each day. Mice could use visual cues to orient themselves,  
175 and to find refuge on a platform submerged ~1.5 cm underneath the water. Because of their aversion  
176 to swimming and the consistent placement of the platform, mice are expected to learn that the platform  
177 is located in the same position relative to directional cues and locate it more quickly over time. We  
178 assessed learning by measuring the distance mice needed to swim to reach the platform, and the  
179 distance it swam in the pool, as well as the percent swim distance in the target quadrant in which the  
180 platform is located. If mice were unable to locate the platform within the allotted time of 1 minute, they  
181 were guided to the platform and allowed to remain there for 10 s. Probe trials were conducted on days  
182 5, 1 h after the last training trial, and then on day 8. During the probe trials the submerged platform  
183 was removed and mice were given 1 min to swim in the pool. Navigation strategies and efficiency were  
184 assessed using traditional measures such as the total swim distance, and the distance spent in each  
185 of the quadrants.

186

187 **2.3 Absolute Winding Number**

188 In addition to the distance metrics traditionally used to describe behavior in the Morris Water Maze  
189 paradigm, we characterized the swim path using a novel metric, the absolute winding number. This is  
190 derived from the well-known winding number in mathematics, is positive-valued and characterizes the  
191 shape of the swimming trajectory, as defined below.

192

193 **2.3.1 Winding Number**

194 Consider a continuous curve  $\gamma \subset \mathbb{R}^2$  defined by the equation

195 
$$\gamma(t) = (x(t), y(t)), t \in [0,1],$$

196 where  $x = x(t)$ ,  $y = y(t)$  are continuous functions, and  $\gamma$  is a closed curve if  $\gamma(0) = \gamma(1)$ . We assume  
197  $\gamma$  does not pass through the origin  $(0,0)$ , and reparametrize the curve in polar coordinates as:

198 
$$\gamma(t) = (r(t)\cos(\theta(t)), r(t)\sin(\theta(t))).$$

199 The winding number of  $\gamma$  is then defined as

200 
$$W_\gamma := \frac{\theta(1) - \theta(0)}{2\pi}.$$

201 For any continuous closed curve, its winding number is always an integer, and measures the total  
202 number of times that curve travels counterclockwise around the origin. The winding number is an  
203 important object of study in differential geometry, complex analysis and algebraic topology.

204

205 **2.3.2 Absolute Winding Number**

206 Our motivation in considering the winding number is to obtain a summary of how much each animal's  
207 movement trajectory deviates from a direct path. However, the winding number is not directly useful  
208 as such a summary for three reasons: (1) the animal tracking data do not directly provide  $\gamma(t)$ , instead  
209 yielding points along the curve at a finite number of times; (2) the curves are not closed as the animals

210 do not return to their starting locations; (3) the movement is not expected to be consistently  
 211 counterclockwise and may change between clockwise and counterclockwise. To address these  
 212 limitations and obtain a more appropriate measure, we propose an Absolute Winding Number (AWN):

213 **Definition 1.** Let  $0 \leq t_0 < t_1 < \dots < t_n$  and  $\gamma_i = \gamma(t_i) = (x(t_i), y(t_i))$ ,  $i = 0, \dots, n$  be discrete points on  
 214 a curve  $\gamma$ , with  $n \geq 3$ . Assume for any  $0 \leq i \leq n - 1$ ,  $\gamma_i \neq \gamma_{i+1}$ , the Absolute Winding Number (AWN)  
 215 of  $\gamma$ , denoted by  $\mathcal{A}_\gamma$ , is defined as  $\mathcal{A}_\gamma := \frac{1}{2\pi} \sum_{i=0}^{n-2} \arccos \left( \frac{(\gamma_{i+2} - \gamma_{i+1})^\top (\gamma_{i+1} - \gamma_i)}{\|\gamma_{i+2} - \gamma_{i+1}\| \|\gamma_{i+1} - \gamma_i\|} \right)$ .

216 The assumption  $\gamma_i \neq \gamma_{i+1}$  means that the animal does not remain at exactly the same location between  
 217 measurement times. The proposed  $\mathcal{A}_\gamma$  is always non-negative, is not necessarily an integer, and  
 218 provides a measure of the degree of deviation of the movement trajectory from a straight line.

219 **Proposition 1.**  $\mathcal{A}_\gamma = 0 \Leftrightarrow \gamma$  is a straight line.

220

221 **2.3.3 Continuous Absolute Winding Number**

222 The AWN in Definition 1 depends on the sampling times  $t_i$ , but provides an estimate approximating a  
 223 continuous AWN (CAWN), which we define below. Let  $\gamma: [0, T] \rightarrow \mathbb{R}^2$  be a plane curve, and consider  
 224 the unit tangent field along  $\gamma$ , denoted by  $X: [0, T] \rightarrow S^1$ , where  $S^1$  is the unit circle, as

225 
$$X(t) = \frac{\gamma'(t)}{\|\gamma'(t)\|} \in S^1.$$

226 Then we represent  $X$  by the circular angle curve  $\theta$ , that is:

227 
$$\theta: [0, T] \rightarrow [0, 2\pi], X(t) = [\cos(\theta(t)), \sin(\theta(t))]^\top.$$

228 The continuous AWN is the length of the curve  $\theta$ :

229 
$$\mathcal{A}_\gamma^c := \frac{1}{2\pi} \int_{[0, T]} \|\theta'(t)\| dt.$$

230 We formulate the continuous analogue of Proposition 1.

231 **Proposition 2.**  $\mathcal{A}_\gamma^c = 0 \Leftrightarrow \gamma$  is a straight line.

232 *Proof.*  $\mathcal{A}_\gamma^c = 0 \Leftrightarrow \theta$  is a constant curve on  $S^1 \Leftrightarrow X$  is a constant vector field  $\Leftrightarrow \gamma$  is a straight line.

233 The following Proposition implies that AWN is a discretization of CAWN: as the sample times  $t_i$  get  
 234 closer and closer together, AWN converges to CAWN:

235 **Proposition 3.** Letting  $\Delta t = \sup_i |t_{i+1} - t_i|$  to be the maximum difference between times, then  
 236  $\lim_{\Delta t \rightarrow 0} \mathcal{A}_\gamma = \mathcal{A}_\gamma^c$ .

237 *Proof.* Given a partition  $0 \leq t_0 < t_1 < \dots < t_n = T$ , observe that

238 
$$\arccos \left( \frac{(\gamma_{i+2} - \gamma_{i+1})^\top (\gamma_{i+1} - \gamma_i)}{\|\gamma_{i+2} - \gamma_{i+1}\| \|\gamma_{i+1} - \gamma_i\|} \right) \approx |\theta(t_{i+1}) - \theta(t_i)|,$$

239 then

240 
$$\mathcal{A}_\gamma \approx \frac{1}{2\pi} \sum_{i=0}^{n-1} |\theta(t_{i+1}) - \theta(t_i)| \rightarrow \frac{1}{2\pi} \int_{[0,T]} |\theta'(t)| dt = \mathcal{A}_\gamma^c.$$

241 **2.3.4 Robustness of the Absolute Winding Number**

242 To characterize errors in tracking movement, suppose we observe  $\xi_i = \gamma_i + \epsilon_i$  with noise  
 243  $\epsilon_i \sim N(0, \sigma^2 Id)$ , where  $Id$  is the two-dimensional identity matrix. We show in Theorem 1 that the estimate  
 244 of AWN based on noisy data,  $\mathcal{A}_\xi$ , is close to the true  $\mathcal{A}_\gamma$  with high probability. This demonstrates  
 245 robustness of the AWN.

246 **Theorem 1.** *Assume there exists  $l_0 > 0$  and  $0 < \varphi_0 < 1$  such that  $\|\gamma_{i+1} - \gamma_i\| \geq l_0$  for  $0 \leq i \leq n-1$   
 247 and  $\left| \frac{(\gamma_{i+2} - \gamma_{i+1})^\top (\gamma_{i+1} - \gamma_i)}{\|\gamma_{i+2} - \gamma_{i+1}\| \|\gamma_{i+1} - \gamma_i\|} \right| \leq 1 - \varphi_0$  for  $0 \leq i \leq n-2$ , then for any  $\delta \leq \min\left\{\frac{l_0}{2}, \frac{l_0 \varphi_0}{2 + \varphi_0}\right\}$ , with probability  $\geq$   
 248  $1 - e^{-\frac{\delta}{8\sigma^2}}$ , we have the following bound:*

249 
$$|\mathcal{A}_\gamma - \mathcal{A}_\xi| \leq \frac{2(n-1)\delta}{\pi(l_0 - \delta) \sqrt{2\left(\varphi_0 - \frac{\delta}{l_0 - \delta}\right)\left(1 - \varphi_0 + \frac{\delta}{l_0 - \delta}\right)}}$$

250 *Proof.* By the definition of AWN and triangular inequality, it suffices to consider a single time interval,  
 251 that is, to compare  $\arccos\left(\frac{(\xi_2 - \xi_1)^\top (\xi_1 - \xi_0)}{\|\xi_2 - \xi_1\| \|\xi_1 - \xi_0\|}\right)$  with  $\arccos\left(\frac{(\gamma_2 - \gamma_1)^\top (\gamma_1 - \gamma_0)}{\|\gamma_2 - \gamma_1\| \|\gamma_1 - \gamma_0\|}\right)$ . To simplify the notation, let  $u_2 = \gamma_2 - \gamma_1$  and  $u_1 = \gamma_1 - \gamma_0$ ,  $\eta_2 = \epsilon_2 - \epsilon_1$ ,  $\eta_1 = \epsilon_1 - \epsilon_0$ . Then we want to analyze:

253 
$$\left| \arccos\left(\frac{(u_2 + \eta_2)^\top (u_1 + \eta_1)}{\|u_2 + \eta_2\| \|u_1 + \eta_1\|}\right) - \arccos\left(\frac{u_2^\top u_1}{\|u_2\| \|u_1\|}\right) \right|. \quad (\text{Eq. 1})$$

254 By the triangular inequality again, (Eq. 1) is upper bounded by  $A + B$  where

255 
$$A = \left| \arccos\left(\frac{(u_2 + \eta_2)^\top (u_1 + \eta_1)}{\|u_2 + \eta_2\| \|u_1 + \eta_1\|}\right) - \arccos\left(\frac{(u_2 + \eta_2)^\top u_1}{\|u_2 + \eta_2\| \|u_1\|}\right) \right|,$$

256 
$$B = \left| \arccos\left(\frac{(u_2 + \eta_2)^\top u_1}{\|u_2 + \eta_2\| \|u_1\|}\right) - \arccos\left(\frac{u_2^\top u_1}{\|u_2\| \|u_1\|}\right) \right|.$$

257 By symmetry, it suffices to bound either term so we focus on B. Let  $f(\eta) := \arccos(\xi_\eta) :=$   
 258  $\arccos\left(\frac{(u_2 + \eta)^\top u_1}{\|u_2 + \eta\| \|u_1\|}\right)$ , then  $B = |f(\eta_2) - f(0)|$ , where  $\eta_2 \sim N(0, 2\sigma^2 Id)$ . Since  $\eta_2 \sim N(0, 2\sigma^2 Id)$ ,  $\frac{\eta_2}{\sqrt{2\sigma^2}} \sim$   
 259  $N(0, 1)$  and  $\frac{\|\eta_2\|^2}{2\sigma^2} \sim \chi(2)$ , then by the tail probability of  $\chi(2)$ , for any  $\delta \leq \min\left\{\frac{l_0}{2}, \frac{l_0 \varphi_0}{2 + \varphi_0}\right\}$ , with probability  
 260 at least  $1 - e^{-\frac{\delta}{8\sigma^2}}$ ,  $\|\eta_2\| \leq \delta$ . Then with high probability, we have the following:

261 
$$\begin{aligned} |\xi_\eta - \xi_0| &\leq \|\nabla_\eta \xi_\eta(\eta)\| \|\eta\| \\ &= \left\| \frac{u_1 \|u_2 + \eta\|^2 \|u_1\| - (u_2 + \eta)^\top u_1 \|u_1\| (u_2 + \eta)}{\|u_2 + \eta\|^3 \|u_1\|^2} \right\| \|\eta\| \\ &\leq \frac{2}{\|u_2 + \eta\|} \|\eta\| \leq \frac{2\delta}{l_0 - \delta}, \end{aligned}$$

262 where the last inequality follows from the assumption  $\|u_2\| \geq l_0$  and  $\|\eta\| \leq \delta \leq \frac{l_0}{2}$ . As a result,

263  $\|\xi_\eta\| \leq \|\xi_0\| + \frac{2\delta}{l_0 - \delta} \leq 1 - \varphi_0 + \frac{2\delta}{l_0 - \delta} = 1 - \varphi,$

264 where  $\varphi = \varphi_0 - \frac{2\delta}{l_0 - \delta} \in (0,1)$  since  $\delta \leq \frac{l_0\varphi_0}{2+\varphi_0}$ . Then we observe that the gradient of  $f$  with respect to  $\eta$   
265 is

266 
$$\nabla_\eta(f)(\eta) = -\frac{1}{\sqrt{1 - \xi_\eta^2}} (\nabla_\eta \xi_\eta(\eta))$$

267 Hence

268 
$$\begin{aligned} \|\nabla_\eta(f)(\eta)\| &\leq \frac{1}{\sqrt{1 - \xi_\eta^2}} \|\nabla_\eta \xi_\eta(\eta)\| \\ &\leq \frac{1}{\sqrt{1 - \xi_\eta^2}} \frac{2}{\|u_2 + \eta\|} \leq \frac{2}{\sqrt{2\varphi - \varphi^2(l_0 - \delta)}}. \end{aligned}$$

269 Finally, we can show:

270 
$$B = |f(\eta_2) - f(0)| \leq \|\nabla_\eta(f)\eta\| \|\eta_2\| \leq \frac{2\delta}{\sqrt{2\varphi - \varphi^2(l_0 - \delta)}}.$$

271 Combining the above inequalities, we have:

272 
$$\begin{aligned} |\mathcal{A}_\gamma - \mathcal{A}_\xi| &\leq \frac{(n-1)}{2\pi} (A + B) = \frac{(n-1)}{\pi} B \\ &\leq \frac{2(n-1)\delta}{\pi(l_0 - \delta)\sqrt{2\varphi - \varphi^2}} \end{aligned}$$

273 with probability at least  $1 - e^{-\frac{\delta}{8\sigma^2}}$  for any  $\delta \leq \min\left\{\frac{l_0}{2}, \frac{l_0\varphi_0}{2+\varphi_0}\right\}$ .

274 The above Theorem implies that the larger  $l_0$  and  $\varphi_0$ , the more robust the AWN. As a result, in practice,  
275 if two consecutive observations  $\gamma_i$  and  $\gamma_{i+1}$  are too close or the inner product between the normalized  
276  $\gamma_{i+1}\gamma_{i+2}$  and  $\gamma_i\gamma_{i+1}$  is very close to 1, then we can remove  $\gamma_{i+1}$  to reduce the impact of random noise.  
277 This is not surprising since if two consecutive observations are almost identical, then tiny noise will  
278 result in huge errors in the angle. Similarly, if the two vectors are almost co-linear, the noise will  
279 contribute more to the true angle, which comes from the fact that the arccos function has infinite  
280 derivative at  $\pm 1$ .

281

282 **2.4 Imaging and Associated Metrics**

283 Diffusion weighted imaging was done using a 9.4T high field MRI, with a 3D SE sequence with TR/TE:  
284 100 ms /14.2 ms; matrix: 420 x 256 x 256; FOV: 18.9 mm x 11.5 mm x 11.5 mm, 45  $\mu\text{m}$  isotropic  
285 resolution, BW 62.5 kHz; using 46 diffusion directions, 2 diffusion shells (23 at 2000, and 23 at 4000  
286  $\text{s/mm}^2$ ); 5 non diffusion weighted (b0). The max diffusion pulse amplitude was 130.57 Gauss/cm;  
287 duration 4 ms; separation 6 ms, 8-fold compressed-sensing acceleration (Wang et al. 2018) (Robert  
288 Anderson 2018) (Uecker M; Ong F; Tamir JI; Bahri 2015). Diffusion data were reconstructed using

289 DIPY (Garyfallidis et al. 2014) with Q-ball Constant Solid Angle Reconstruction, producing ~2 million  
290 tracts. We have used pipelines implemented in a high-performance computing environment, to  
291 segment the brain in sub regions (Anderson et al. 2019). We focused on a subset including the  
292 hippocampus, caudate-putamen, and their main connections, the fimbria and fornix, and the internal  
293 capsule, as well as the cerebellar white matter. For these regions we calculated features including  
294 volume and microstructural properties like fractional anisotropy (FA), to reconstruct tracts and build  
295 connectivity matrices. We used the Brain Connectivity toolbox (Rubinov and Sporns 2010) to calculate  
296 degree of connectivity (DEG) and clustering coefficient (CLUS) for the hippocampus and caudate  
297 putamen and associated fiber tracts, including fimbria (fi) and fornix (fx) for the hippocampus (Hc), and  
298 internal capsule (ic) for the caudate putamen (CPu), respectively as well as the cerebellar white matter  
299 (cbw).

300

## 301 **2.5 Statistical Analyses**

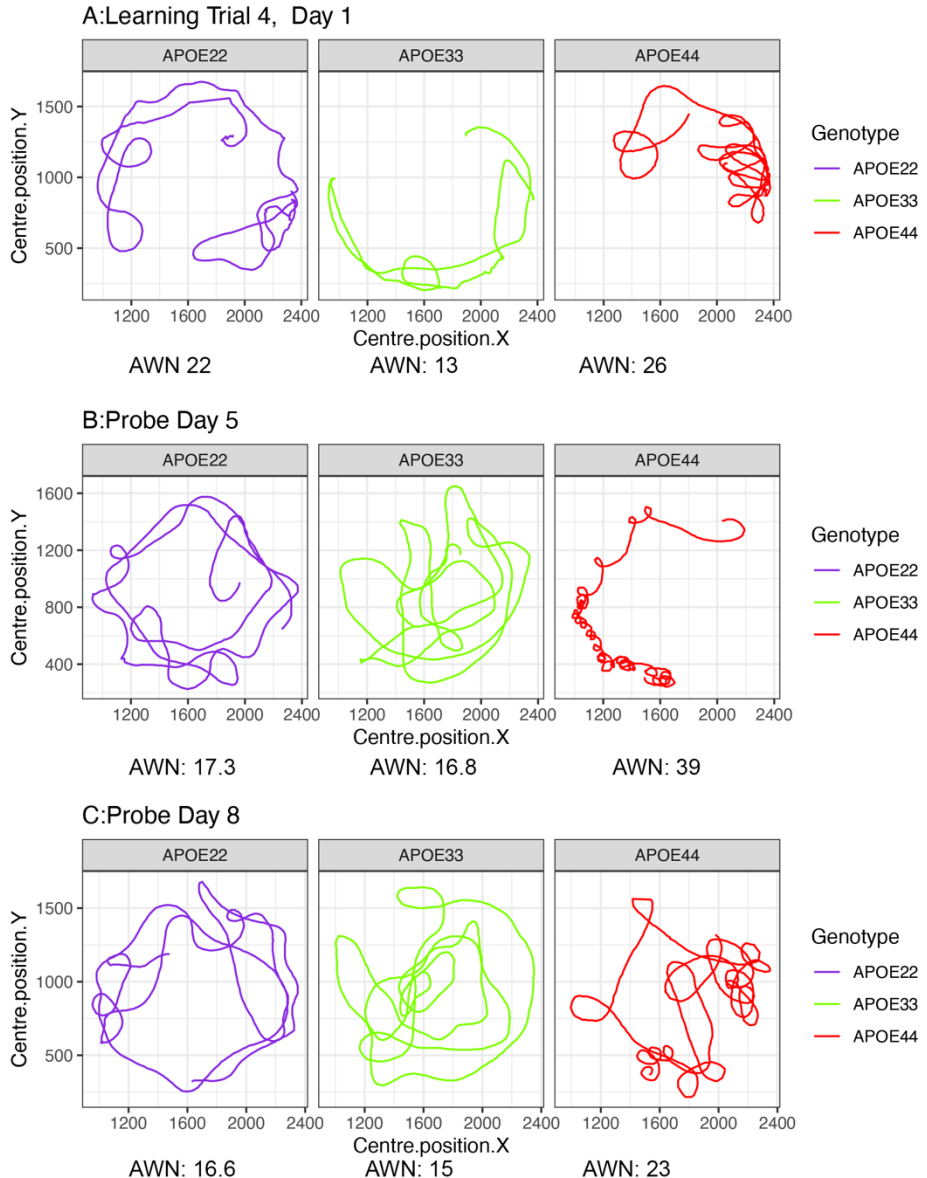
302 Statistical analyses were conducted in R to build linear models, and apply ANOVA analyses to  
303 determine the effects of genotype and sex on the behavioral markers of interest, including the total  
304 swim distance, normalized swim distance in the target quadrant, and the absolute winding number  
305 introduced above. The ANOVA analyses were followed by post hoc tests (using Sidak adjustments),  
306 and  $p < 0.05$  was considered significant. We similarly analyzed the regional volumes and FA, as well  
307 as the degree of connectivity and clustering coefficient. We used the emtrends function (emmeans R  
308 package), and evaluated linear models to relate behavioral metrics to the imaging and connectivity  
309 markers to understand if they influence the AWN, and if different genotypes/sexes use preferentially  
310 different circuits.

311

## 312 **3 Results**

### 313 **3.1 Swim Paths**

314 A qualitative analysis revealed that swim paths for selected individuals from each of the three  
315 genotypes, differed in length and shape for the learning trials and the probe tests administered in day  
316 5, 1 hour after the trials ended, and on day 8. The last trial of day 1 is shown in **Figure 1**, since animals  
317 are likely to swim for ~1 minute during the first day (A), and this is the same duration as in the probe  
318 tests, shown in (B) and (C).



319

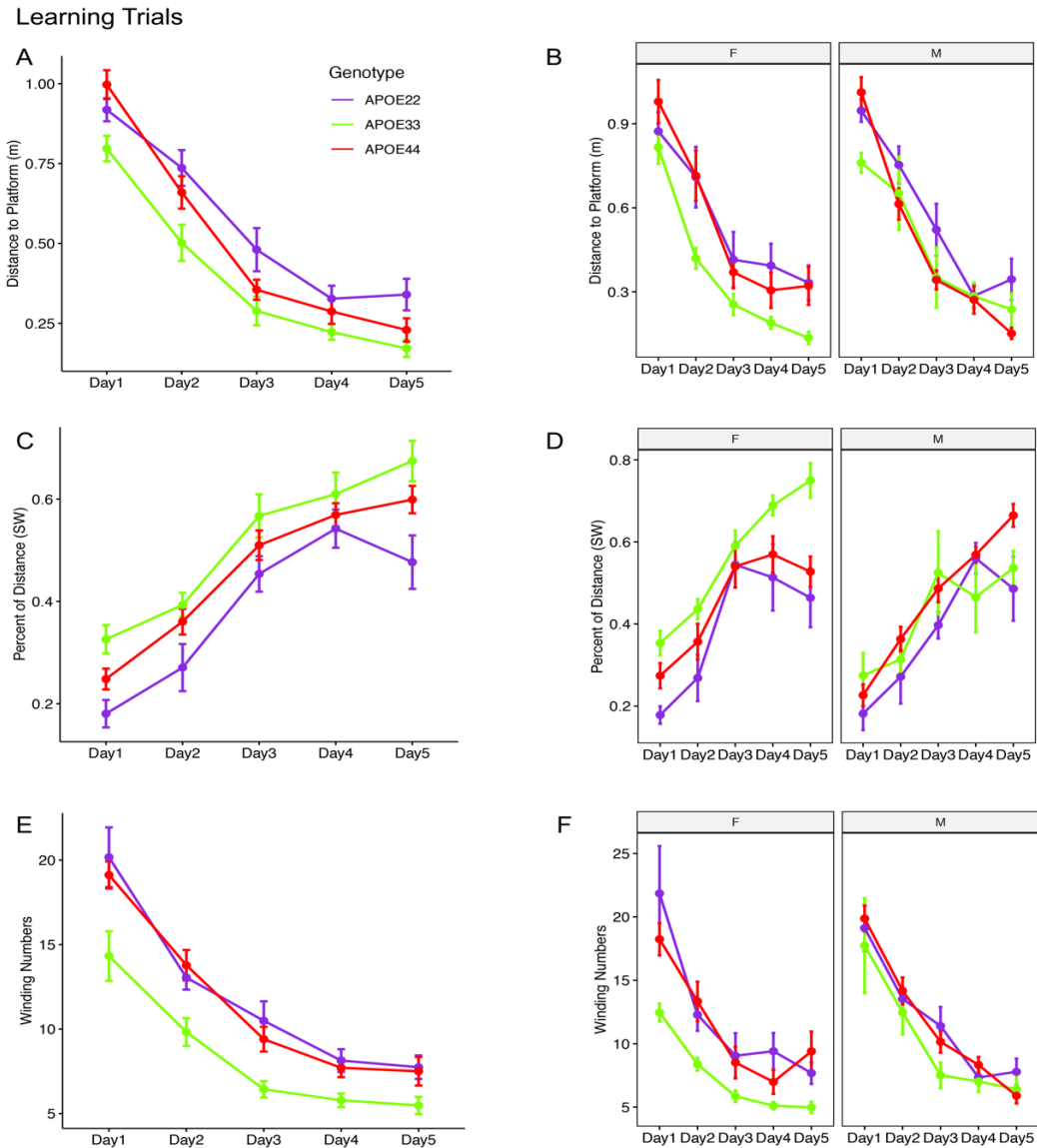
320 **Figure 1. Examples of swim paths shapes for animals with APOE2, APOE3, and APOE4**  
321 **genotypes.** Qualitative observations suggest that swim paths differed not just in length, but also in  
322 shape. Trajectories are presented for the last trial in day 1 (A), probe in day 5 (B) and probe in day 8  
323 (C). We chose animals illustrating medium (APOE2: learning=22, d5=17.3; d8=16.6), medium-small  
324 (APOE3: learning=13, d5=16.8, d8=15), and large winding numbers (APOE4: learning=26, d5=39;  
325 d8=23). APOE22: homozygous for APOE2; APOE33: homozygous for APOE3; APOE44: homozygous  
326 for APOE4.

327

### 328 **3.2 Learning Trials**

329 An ANOVA analysis for the total distance to the platform (**Figure 2 A, B**) revealed a significant effect  
330 of time ( $F(4,240)=128.2$ ,  $p=2.2*10^{-16}$ ), genotype ( $F(2,262)=15.9$ ,  $p<3.2*10^{-7}$ ), and a significant  
331 interaction of genotype by sex ( $F(2,262)=4.2$ ,  $p=0.02$ ). Post hoc tests indicated that differences within

332 female groups were significant for APOE2 versus APOE3 genotypes ( $t=4.1$ ,  $p=1.9*10^{-4}$ ), as well as  
 333 between APOE3 and APOE4 genotypes ( $t=-4.9$ ,  $p<10^{-5}$ ). The differences within male groups were  
 334 significant for APOE2 versus APOE3 genotypes ( $t=2.5$ ,  $p=0.03$ ), as well as between APOE2 versus  
 335 APOE4 genotypes ( $t=2.5$ ,  $p=0.04$ ). Differences were larger between females, and only APOE4 females  
 336 were different relative to APOE3 females, but this was not true for males of the same genotypes. Sex  
 337 differences were significant for APOE3 mice ( $t=-2.2$ ,  $p=0.03$ ), and showed a trend for APOE4 mice  
 338 ( $t=1.75$ ,  $t=0.08$ ).



339

340 **Figure 2. Learning trials.** Mice swam shorter distances over the 5 testing days until reaching the  
 341 hidden platform, indicating that they were learning. Meanwhile, the percentage time swam in the target  
 342 quadrant increased with time. The absolute winding number clearly discriminated the APOE3 mice  
 343 relative to APOE2 and APOE4 carriers, which used more similarly shaped trajectories. The effects  
 344 were larger in females across the 5 days. F: female; M: male. Graphs show mean±standard error.

345 An ANOVA analysis for the normalized distance swam in the target (SW) quadrant (**Figure 2 C, D**)  
 346 revealed that there was a significant effect of time ( $F(4,232)=69.8$ ,  $p=2.6*10^{-16}$ ) and genotype

347 (F(2,232)=13.6, p<2.6\*10<sup>-6</sup>), a significant interaction of genotype by sex (F(2,232)=8.5, p=0.0003), and  
348 a trend for the interaction of genotype by sex by time (F(8,232)=1.9, p=0.06). Post hoc tests indicated  
349 that differences within female groups were significant for APOE2 versus APOE3 genotypes (t=-4.9,  
350 p<10<sup>-4</sup>), as well as between APOE3 and APOE4 genotypes (t=4.5, p<10<sup>-4</sup>). Post hoc tests indicated  
351 that differences within male groups were significant for APOE2 versus APOE4 genotypes (t=-2.5  
352 p=0.03). Sex differences were significant for APOE3 mice (t=4.8, p=2.2\*10<sup>-6</sup>). Differences between  
353 APOE3 and APOE4 mice could thus be largely attributed to differences in females.

354 A qualitative evaluation of the absolute winding number indicated more similar swim trajectories  
355 between APOE2 and APOE4 mice, and a clear demarcation relative to APOE3 mice. Moreover, these  
356 differences appeared clearer in females. An ANOVA analysis (**Figure 2 E, F**) revealed a significant  
357 effect of time (F(4,240)=86.9, p=2.2\*10<sup>-16</sup>), and genotype (F(2,240)=24.15, p<2.8\*10<sup>-10</sup>), as well as a  
358 significant effect of sex, that was not captured by the previous metrics (F(1,240)=4.8, p=0.03). There  
359 was also a significant interaction of genotype by sex (F(2,240)=3.9, p=0.02), while the time by sex  
360 interaction was characterized by F(4,240)=1.7, p=0.16. Post hoc tests indicated that differences within  
361 females were significant for APOE2 versus APOE3 genotypes (t=5.4, p<10<sup>-5</sup>), as well as between  
362 APOE3 and APOE4 genotypes (t=-5.7, p<10<sup>-5</sup>). Differences within males were not significant. Thus,  
363 differences in the shape of the trajectories were explained by females. Sex differences were significant  
364 for APOE3 mice (t=-3.5, p=0.0006).

365 The absolute winding number better discriminated APOE3 mice relative to APOE2 and APOE4 mice,  
366 which performed more similarly in terms of their spatial navigation strategy.

367

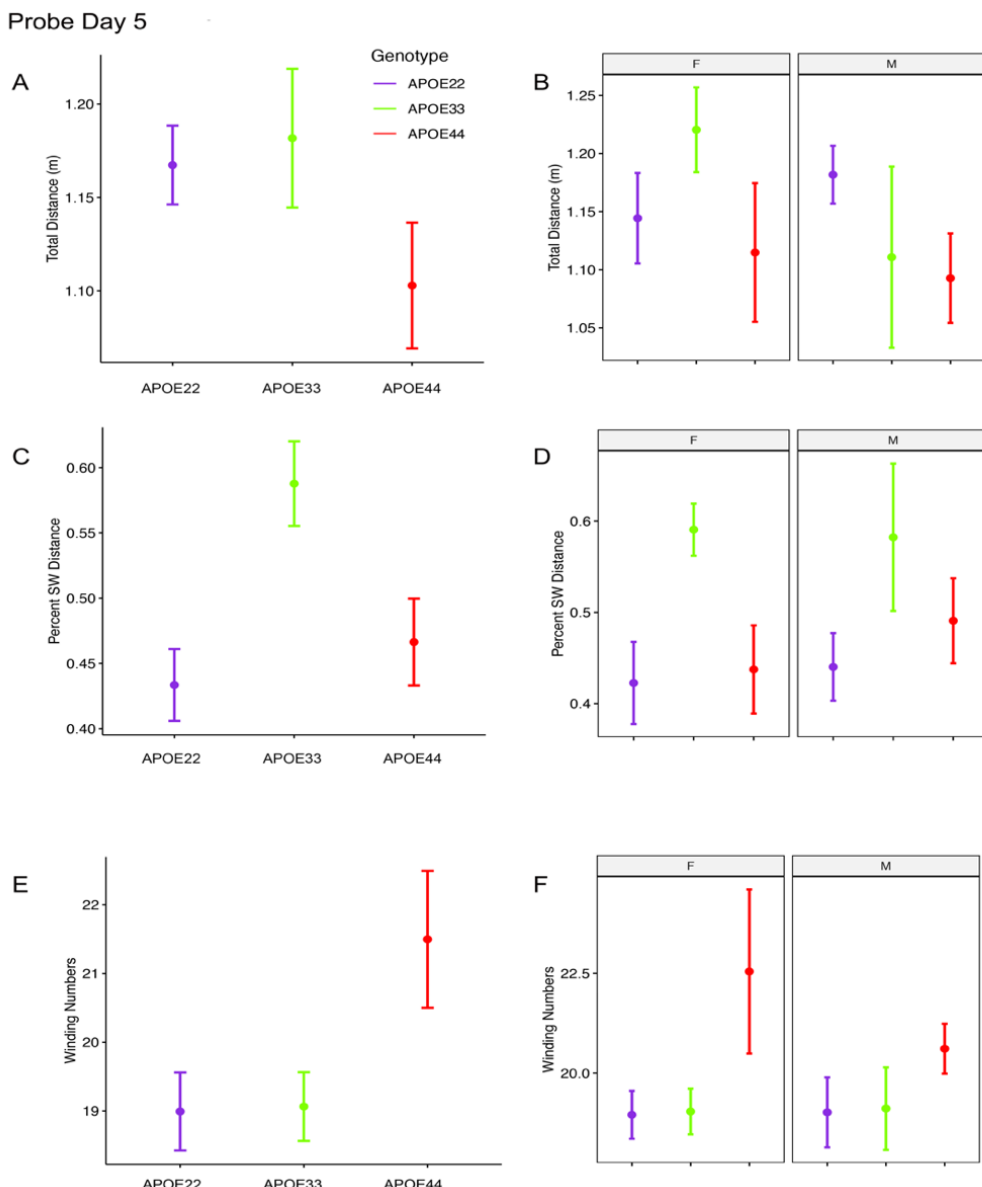
### 368 **3.3 Probe Trials – Long Term Memory**

369 An ANOVA analysis for the total distance swam during the probe trial (1 minute) administered on day  
370 5 (**Figure 3**), one hour after the last learning trial did not detect significant differences.

371 The percent distance swam in the target quadrant during this probe on day 5 showed a significant  
372 effect of genotype (F(2,48)=4.5, p=0.02). Post hoc tests within groups of females (Sidak corrected)  
373 indicated significant differences within females showed a significant difference between APOE3 and  
374 APOE4 mice (t=2.5, p=0.04). Differences within groups of male mice were not significant.

375 The absolute winding number during day 5, testing long term memory, identified borderline significant  
376 differences due to APOE genotype (F(2,48)=3.02, p=0.06). These differences were found between  
377 females of APOE4 genotypes relative to APOE3 genotypes (t=-2.3, p=0.07). Differences within groups  
378 of male mice were not significant.

379



380

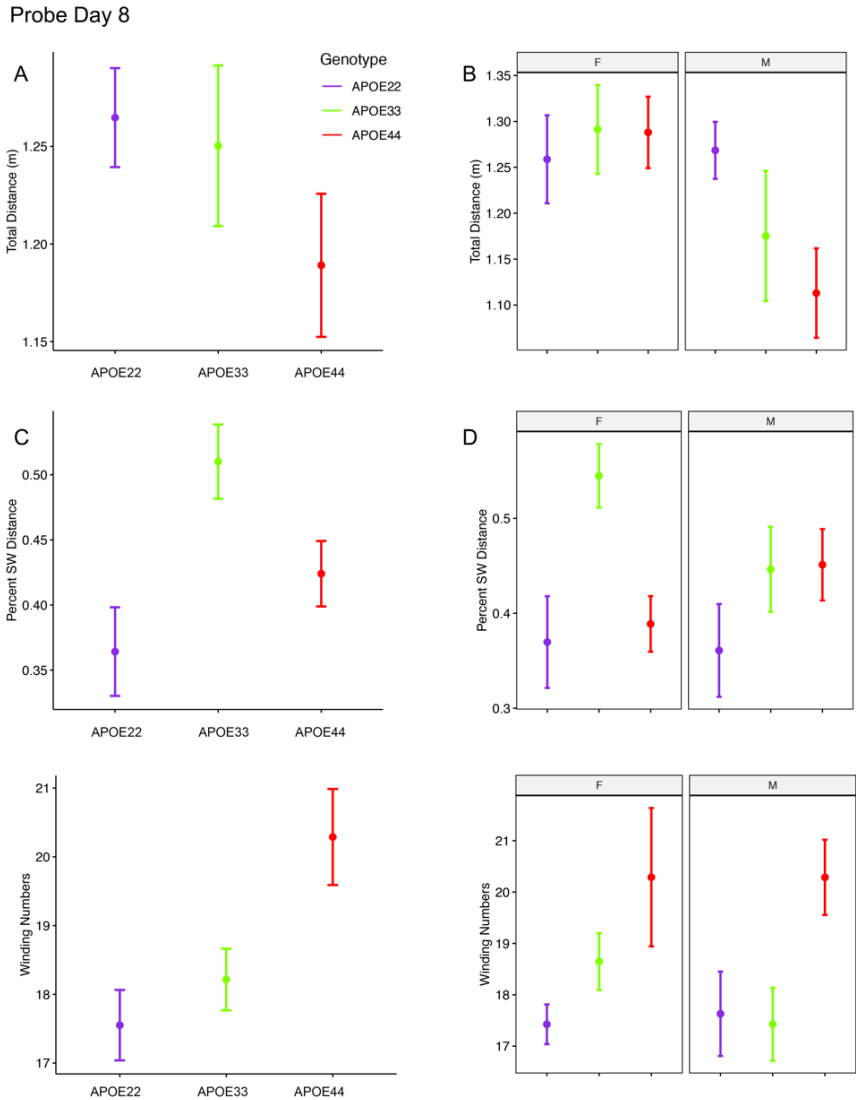
381 **Figure 3. Probe trials 1 hour after ending the learning trials.** Long term memory tested one hour  
382 after the end of learning trials indicated that APOE4 mice swam less than APOE2 and APOE3 mice,  
383 and the data suggested a “dose dependent” genotype effect in males. APOE3 mice spent most of their  
384 swimming in the target quadrant (~80%), while APOE2 and APOE4 mice spent (~50%) of their  
385 swimming in the target quadrant, but the differences between males and females were not significant.  
386 APOE2 and APOE4 mice were more similar, while significant differences were noticed between  
387 APOE2 and APOE3 mice, as well as between APOE3 and APOE4 female mice. The shape of the  
388 swim path, described by the absolute winding number showed similarities between APOE2 and  
389 APOE3 mice, but higher loopiness for APOE4 mice. These differences were largest for females. F:  
390 female; M: male. Graphs show mean±standard error.

391

392 An ANOVA analysis for the total distance swam during the 1 minute of the probe trial administered on  
393 day 8 (**Figure 4**), 3 days after the last learning trial, indicated a significant effect of sex ( $F(1,47)=7.3$ ,

394 p=0.01). Post hoc tests within groups of males (Sidak corrected) indicated borderline differences  
395 between APOE2 and APOE4 genotypes ( $t=2.36$ ,  $p=0.06$ ). Differences between males and females of  
396 the same genotypes were found for APOE4 mice ( $t=2.8$ ,  $p=0.007$ ).

397



398

399 **Figure 4. Probe trials 3 days after ending the learning trials (mean±standard error).** A. The largest  
400 effects in terms of total distance were seen in males, where APOE4 mice swam the shortest distances.  
401 Our analysis does not capture stops when animals may orient themselves. B. The percentage time  
402 swam in the target quadrant was largest in APOE3 mice relative to APOE2 and APOE4 mice. This  
403 effect was driven largely by females, while male mice with APOE2 genotype spent less time in the  
404 target quadrant relative to other mice, and APOE3 and APOE4 mice performed similarly. A dose  
405 dependent effect was apparent in the absolute winding number for all genotypes, and this was reflected  
406 mostly in females. Male mice with APOE2 and APOE3 genotypes used similar strategies, females with  
407 APOE2 genotypes having smaller winding numbers. APOE4 males had loopier swim trajectories  
408 relative to both APOE2 and APOE3 mice, which had similar trajectories. F: female; M: male. Graphs  
409 show mean±standard error.

410 The percent distance swam in the target quadrant during this probe on day 8 showed a significant  
411 effect of genotype ( $F(2,47)=5.0$ ,  $p=0.01$ ), and a trend for the interaction of genotype by sex

412 (F(2,47)=2.3, p=0.1). Post hoc tests within groups of females (Sidak corrected) indicated significant  
413 differences between APOE2 and APOE3 mice ( $t=-2.7$ ,  $p=0.03$ ), and between APOE3 and APOE4  
414 ( $t=3.1$ ,  $p=0.01$ ). Differences within groups of male mice were not significant. Differences between  
415 males and females of the same genotypes showed a trend only, for APOE3 mice ( $t=1.7$ ,  $p=0.1$ ).

416 The winding number for the probe in day 8 showed a significant effect of genotype ( $F(2,47)=5.3$ ,  
417  $p=0.008$ ). While differences within females were not significant, our data suggests a “dose” effect  
418 APOE2<APOE3<APOE4. Post hoc tests within groups of males showed borderline differences  
419 between APOE2 and APOE4 mice ( $t=-2.2$ ,  $p=0.08$ ) mice, and between APOE3 and APOE4 mice ( $t=-$   
420  $2.2$ ,  $p<0.09$ ).

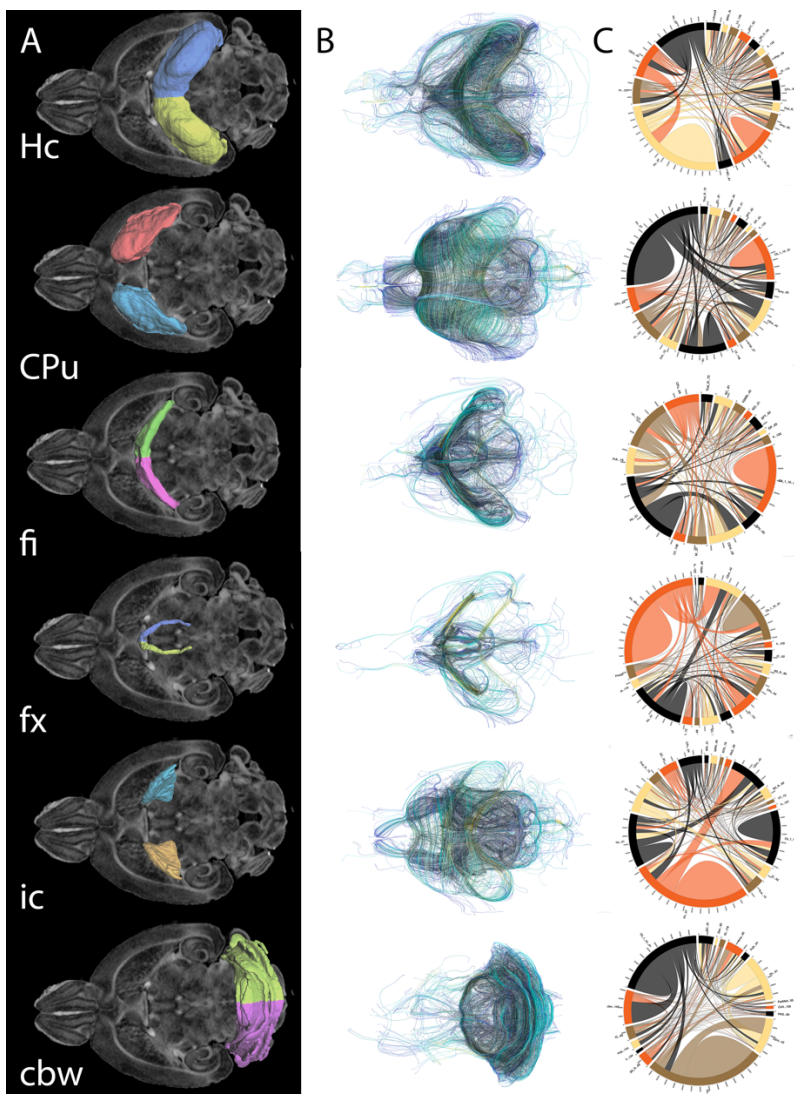
421 Thus, the absolute winding numbers indicated more complex trajectories for APOE4 mice relative to  
422 APOE3 and APOE2 mice.

423

424 **3.4 MRI Correlates of Spatial Navigation**

425 As both the hippocampus and caudate putamen have been involved in spatial navigation, we examined  
426 imaging markers corresponding to changes in navigation strategies based on volume, fractional  
427 anisotropy, and structural connectivity (**Figure 5**) of these major gray matter regions, and their main  
428 white matter connections, i.e. fimbria, and fornix for the hippocampus, and the internal capsule for the  
429 caudate putamen. We have also examined the cerebellar white matter due to its less understood role,  
430 its involvement in spatial navigation, and potential hippocampal cerebellar connections (Rochefort,  
431 Lefort, and Rondi-Reig 2013).

432



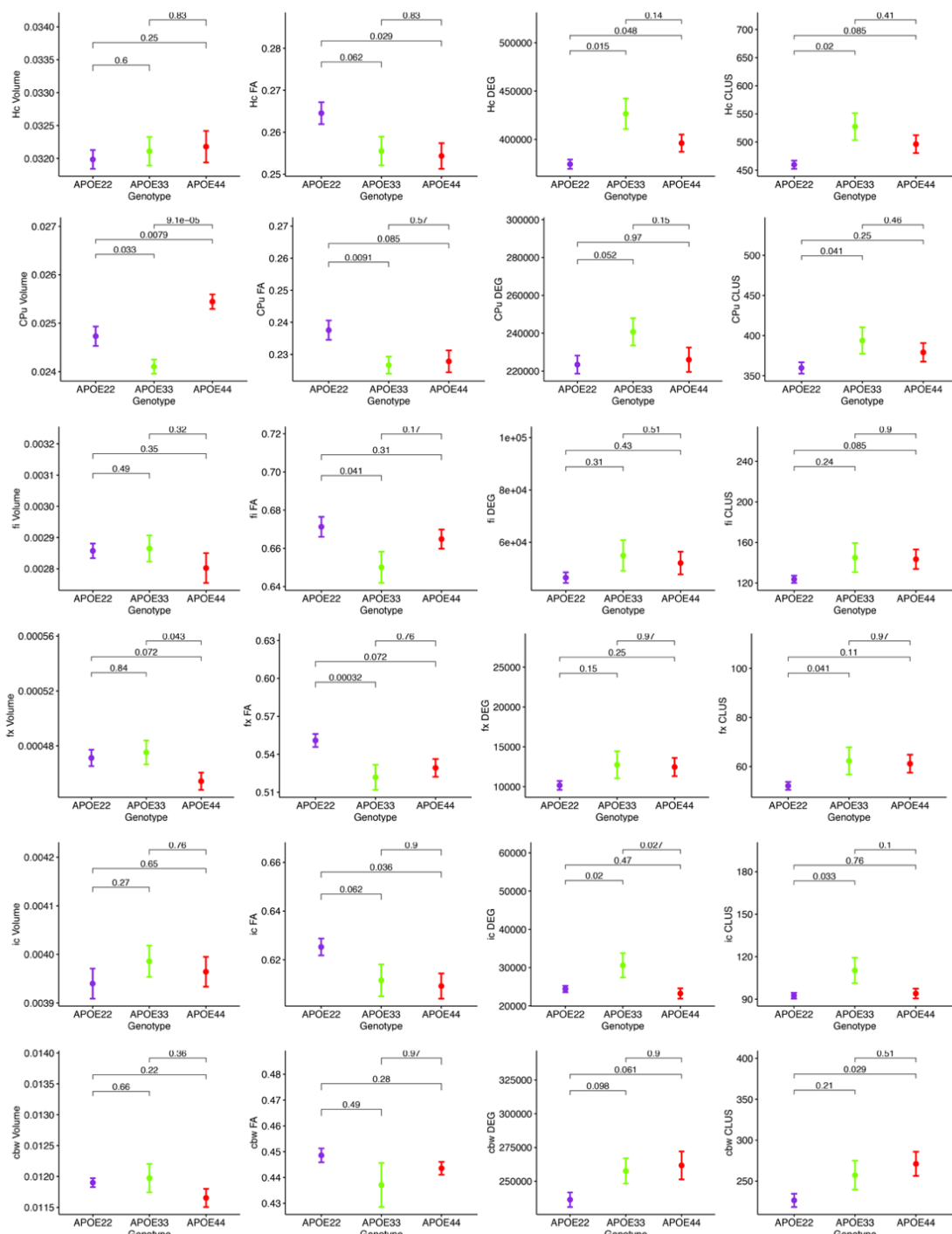
433

434

435 **Figure 5. Regions of interest for spatial navigation and their MRI associated metrics.** We  
436 segmented selected brain regions involved in spatial navigation, including the hippocampus (Hc),  
437 caudate putamen (CPu), and their major connections (fimbria: fi, and fornix: fx; and internal capsule :  
438 ic, respectively), to which we added the cerebellar white matter, and we have measured their volumes  
439 (A). These regions were characterized by diffusion based measurements, which characterize  
440 microstructure through texture, and may vary along tracts (such as fractional anisotropy) (B). Finally  
441 we characterized their connectivity with other brain regions (C). Abbreviations and region indices  
442 correspond to the CHASS atlas (Calabrese et al. 2015),(Anderson et al. 2019) and Paxinos mouse  
443 brain atlas: Hc: hippocampus; CPu: caudate putamen, fi: fimbria, fx: fornix, ic: internal capsule, cbw:  
444 cerebellar white matter.

445

446 MRI regional metrics for all three genotypes are shown in **Figure 6**, and summarized in **Table 2**.



447

448 **Figure 6. Imaging and network markers for volume, FA, degree of connectivity and clustering**  
449 **coefficient showed APOE genotype differences.** Graphs show mean $\pm$ standard error.

450

451

Region	Volume		FA		DEG		CLUS	
	F	p	F	p	F	p	F	p
Hc	0.43	0.63	4.11	0.03*	6.9	0.005*	4.34	0.03*
CPu	13.82	0.0001*	3.97	0.03*	2.03	0.15	2.04	0.15
fi	0.86	0.43	2.92	0.07	1.12	0.53	1.62	0.22
fx	3.03	0.07	5.27	0.01*	1.56	0.23	2.3	0.12
ic	0.46	0.62	5.51	0.01*	5.99	0.008*	4.53	0.02*
cbw	2.78	0.08	1.99	0.16	2.75	0.09	2.99	0.07

452

453 **Table 2. APOE genotype differences in MRI metrics i.e. volume, fractional anisotropy (FA),**  
 454 **degree of connectivity (DEG), and clustering coefficient (CLUS)** for regions of interest including:  
 455 hippocampus (Hc), caudate putamen (CPu), fimbria (fi), fornix (fx), internal capsuel (ic), and cerebellar  
 456 white matter (cbw).

457

#### 458 **Hippocampus**

459 An ANOVA analysis of hippocampal volume did not show an effect of genotype, but a significant  
 460 effect of sex ( $F(1,23)=19.0$ ,  $p=0.0002$ ). There were significant effects within all the genotypes APOE2  
 461 ( $t=-2.4$ ,  $p=0.02$ ), APOE3 ( $t=-2.9$ ,  $p=0.008$ ), APOE4 ( $t=-2.3$ ,  $p=0.03$ ). Differences between males and  
 462 females were significant within APOE2 mice ( $t=-2.4$ ,  $p=0.02$ ), APOE3 mice ( $t=-2.9$ ,  $p=0.008$ ), and  
 463 APOE4 mice ( $t=-2.3$ ,  $p=0.03$ ).

464 FA only showed a significant effect of genotype ( $F(2,23)=4.1$ ,  $p=0.03$ ), and a trend for the genotype by  
 465 sex interaction ( $F(2,23)=2.4$ ,  $p=0.1$ ). Significant differences were found only within groups of females:  
 466 APOE2 versus APOE3 ( $t=2.7$ ,  $p=0.03$ ), and APOE2 versus APOE4 ( $t=3.2$ ,  $p=0.009$ ). Differences  
 467 between groups of males were not significant. Sex differences between animals of the same genotype  
 468 were borderline significant for APOE4 mice, but not for the other genotypes ( $t=-1.7$ ,  $p=0.1$ ).

469 The clustering coefficient showed a significant effect of genotype ( $F(2,23)=6.9$ ,  $p=0.004$ ), and a trend  
 470 for sex ( $F(1,23)=2.8$ ,  $p=0.1$ ). Interestingly, differences were significant between males of APOE2 and  
 471 APOE3 genotypes ( $t=-2.7$ ,  $p=0.03$ ). There were no differences between males and females of the  
 472 same genotype.

473

#### 474 **Caudate Putamen**

475 The ANOVA analysis for the caudate putamen showed a singificant effect of genotype ( $F(2,23)=13.8$ ,  
 476  $p=0.0001$ ). Differences between groups of females were significant for APOE2 versus APOE4 mice  
 477 ( $t=-2.8$ ,  $p=0.02$ ), and between APOE3 and APOE4 mice ( $t=-4.4$ ,  $p<0.001$ ). Differences between groups  
 478 of males were only significant between APOE3 and APOE4 mice ( $t=-2.9$ ,  $p=0.02$ ). Differences between  
 479 males and females within the same genotypes were borderline significant for APOE4 mice ( $t=1.7$ ,  
 480  $p=0.1$ ).

481 FA analyses indicated a significant effect of genotype ( $F(2,23)=3.9$ ,  $p=0.03$ ), and differences within  
 482 groups of females were borderline significant for APOE2 versus APOE4 ( $p=2.4$ ,  $p=0.06$ ). Also  
 483 differences between male and female AP0E44 mice were borderline significant ( $t=-1.9$ ,  $p=0.07$ ).

484 We did not detect significant differences in the degree and clustering coefficient of the caudate  
485 putamen.

486

487 **Fimbria and Fornix**

488 The fimbria volume was borderline significant for the interaction term genotype by sex ( $F(2,23)=2.6$ ,  
489  $p=0.1$ ). The FA only showed a trend for genotype ( $F(2,23)=2.9$ ,  $p=0.1$ ). We did not detect significant  
490 differences in the clustering coefficient. The ANOVA analyses for the fornix did not show an effect for  
491 genotype and sex.

492

493 **Internal Capsule**

494 We found no differences in the volume of the internal capsule, however the FA showed a significant  
495 effect of genotype ( $F(2,23)=5.5$ ,  $p=0.01$ ), as well as sex ( $F(1,23)=17.7$ ,  $p=0.0003$ ). Within groups of  
496 females, differences between APOE2 and APOE4 mice were significant ( $t=3.1$ ,  $p=0.01$ ), and showed  
497 a trend between APOE2 and APOE3 mice ( $t=2.5$ ,  $p=0.05$ ). We found no significant differences  
498 between groups of males of different genotypes. An analysis within genotypes showed differences  
499 between APOE3 mice of different sexes ( $t=-2.5$ ,  $p=0.02$ ), and between APOE4 mice of different sexes  
500 ( $t=-3.9$ ,  $p=0.002$ ).

501 The degree of connectivity showed significant effects for genotype ( $F(2,23)=6$ ,  $p=0.008$ ), sex  
502 ( $F(1,23)=5.7$ ,  $p=0.03$ ) and the interaction of genotype by sex ( $F=3.6$ ,  $p=0.045$ ). Within groups of  
503 females we identified differences between APOE2 and APOE3 mice ( $t=-3.8$ ,  $p=0.003$ ), and APOE3  
504 and APOE4 mice ( $t=4.1$ ,  $p=0.001$ ). These differences were not seen within groups of males.  
505 Differences between males and females were only identified for APOE3 mice ( $t=3.5$ ,  $p=0.002$ ).

506 Similar differences as for the degree of connectivity we noticed for the clustering coefficient, showing  
507 significant effects for genotype ( $F(2,23)=4.5$ ,  $p=0.02$ ), sex ( $F(1,23)=5.0$ ,  $p=0.03$ ), but the interaction  
508 between genotype and sex was not significant. Within groups of females we identified differences  
509 between APOE2 and APOE3 mice ( $t=-3.4$ ,  $p=0.007$ ), and between APOE3 and APOE4 mice ( $t=3.1$ ,  
510  $p=0.01$ ). These differences did not persist within groups of males. Differences between males and  
511 females were only found for APOE3 mice ( $t=2.9$ ,  $p=0.008$ ).

512

513 **Cerebellar White Matter**

514 For volume, we only identified a trend for the genotype effect ( $F(2,23)=2.8$ ,  $p=0.08$ ), but a significant  
515 effect of sex ( $F(1,23)=18.9$ ,  $p=0.0002$ ), and for the genotype by sex interaction ( $F(2,23)=7.9$ ,  $p=0.002$ ).  
516 Post hoc tests identified significant differences between females of APOE2 and APOE3 genotypes ( $t=-$   
517  $3.5$ ,  $p=0.005$ ), and between females of APOE3 and APOE4 genotypes ( $t=3.1$ ,  $p=0.01$ ). For male mice  
518 differences were significant between APOE2 and APOE4 mice ( $t=3.1$ ,  $p=0.01$ ). For mice of the same  
519 genotypes sex differences were significant for APOE3 ( $t=4.9$ ,  $p=5.6*10^{-5}$ ), and also for APOE4 mice  
520 ( $t=3.2$ ,  $p=0.004$ ).

521 FA showed a significant interaction between genotype and sex ( $F(2,23)=5.3$ ,  $p=0.01$ ). Within groups  
522 of females APOE2 and APOE3 showed significant differences ( $t=3.8$ ,  $p=0.002$ ), and a trend for APOE3  
523 and APOE4 mice ( $t=-2.4$ ,  $p=0.06$ ). Sex differences were identified for APOE3 mice only.

524

525 The degree of connectivity only showed a trend for the effect of genotype ( $F(3,23)=2.7$ ,  $p=0.1$ ), and  
526 this paralleled our results for the clustering coefficient, which showed a trend for the genotype effect  
527 ( $F(2,23)=3.0$ ,  $p=0.07$ ).

528 In conclusion, genotype differences were noted for the volume of the caudate putamen, the FA of the  
529 hippocampus, caudate putamen, fimbria and fornix, and the connectivity of the hippocampus and  
530 internal capsule.

531

### 532 **Spatial navigation trajectory shape as a function of imaging parameters**

533 We built linear models for the AWN during the two probes for the hippocampus, caudate putamen, and  
534 their connecting tracts, as well as the cerebellar white matter and assessed the significance of the  
535 relationships between AWN and regional imaging metrics for all mice (**Table 3**).

Day5			
Region	Metric	F	p
CPu	Volume	9.86	0.006*
fi	Volume	17.81	0.0006*
Hc	FA	5.23	0.02*
CPu	FA	4.51	0.048*
ic	FA	7.77	0.02*
fx	FA	4.003	0.06

Day8			
Region	Metric	F	p
CPu	Volume	42.25	5.45E-06*
fx	Volume	10.61	0.005*
Hc	FA	10.15	0.005*
fx	FA	5.39	0.03*
ic	FA	12.61	0.002*
fi	DEG	2.96	0.1
fx	DEG	5.35	0.03*
ic	DEG	7.35	0.02*
fi	CLUS	5.78	0.03*
fx	CLUS	4.85	0.04*
cbw	CLUS	6.06	0.03*
CPu	FA	3.8	0.07

536 **Table 3. Main ANOVA results on the linear models predicting AWN based on MRI metrics.**

537

538 We examined whether the relationships between AWM and imaging metric differed for mice of different  
539 genotypes and sexes (**Table 4**, **Figure 7** and **Figure 8**).

540

541 **Hippocampus:**

542 **Day 5.** There was a significant effect of the FA on the absolute winding number for day 5 ( $F(1,7)=7.3$ ,  
543  $p=0.02$ ). Differences between female groups were borderline significant ( $F(1,7)=4.8$ ,  $p=0.07$ ).

544 There was a trend for the interaction between the degree of connectivity and genotype ( $F(2,17)=2.5$ ,  
545  $p=0.1$ ). Also, there was a trend within males ( $F(1,10)=4.6$ ,  $p=0.06$ ). There was a trend for the slopes  
546 differences between APOE3 and APOE4 females ( $t=1.1$ ,  $p=0.1$ , and between males and females  
547 APOE3 carriers ( $t$  ratio =2.1,  $p=0.05$ ). There was a significant effect for the clustering coefficient as a  
548 predictor for the winding number at day 5 for males ( $F(1,10)=5.1$ ,  $p<0.05$ ), a trend for APOE3 females  
549 ( $t$  ratio 1.58,  $p=0.1$ ), and for the differences between slopes for males and female APOE3 ( $t=1.8$ ,  
550  $p=0.09$ ).

551 **Day 8.** There was a significant effect of FA ( $F(2,17)=10.2$ ,  $p=0.005$ ), and a trend for sex ( $F(1,17)=3.07$ ,  
552  $p=0.1$ ), and the interaction FA by sex ( $F(1,17)= 4.22$ ,  $p=0.06$  ). The efect was significant within females  
553 ( $F(1,7)=12.1$ ,  $p=0.01$ ). There was a trend for slope differences between females and males of APOE2  
554 genotypes ( $t$  ratio=-2,  $p=0.07$ ), and APOE4 ( $t$  ratio=-2,  $p=0.08$ ). There was only a trend for the degree  
555 of connectivity interaction by sex  $F(1,17)=2.9$ ,  $p=0.1$ . The slopes were different between males and  
556 females APOE3 mice ( $t$  ratio 2.4,  $p=0.03$ ).

557

558 **Caudate Putamen:**

559 **Day 5.** There was a significant effect of volume on the winding number at day 5 ( $F(1,17)=9.9$ ,  $p=0.006$ ).  
560 The effect within females was characterized by  $F(1,7)=5.5$ ,  $p=0.05$ .

561 There was also a significant effect of FA on the absolute winding number ( $F(1,17)=4.5$ ,  $p<0.05$ ), and  
562 for the interaction of FA with sex ( $F(1,17)=4.47$ ,  $p<0.05$ ). There was a significant effect of FA on AWN  
563 within females ( $F(1,7)=6.5$ ,  $p=0.04$ ), and a trend for slopes differences between males and females  
564 with APOE4 genotypes ( $t$  ratio =-2.0,  $p=0.06$ ).

565 The degree of connectivity showed a significant effect as a predictor within males ( $F(1,10)=7$ ,  $p=0.02$ ).  
566 This was paralelled by the clustering coefficient showing as a significant predictor within males  
567 ( $F(1,10)=10.4$ ,  $p=0.009$ ). There was a trend for slopes differences between females and males of  
568 APOE3 genotypes ( $t$  ratio =1.7,  $p=0.1$ ).

569 **Day 8.** There was a significant effect of the CPu volume on the AWS  $F(1,17)=42.3$ ,  $p=5*10^{-6}$ ), and the  
570 effect was significant both within males ( $F(1,10)=8.2$ ,  $p=0.02$ ), and within females  $F(1,7)=34.7$ ,  
571  $p=0.006$ ). There was a difference between slopes for APOE3 males and females ( $t$  ratio=2.3,  $p=0.03$ ).

572 There was a significant effect of FA within females only ( $F(1,7)=11.8$ ,  $p=0.01$ ).

573 There was a significant effect of the degree of connectivity both withing males ( $F(1,10)=7.7$ ,  $p=0.02$ ),  
574 and females ( $F(1,7)=6.5$ ,  $p=0.04$ ). The slopes were different within APOE3 mice ( $t$  ratio=2.2,  $p=0.04$ ),  
575 and showed a trend within APOE2 mice ( $t$  ratio=1.7,  $p=0.1$ ).

576 There was a significant difference in slopes for the AWN versus CPu clustering coefficient between  
577 APOE3 male and female mice ( $t$  ratio=2.4,  $p=0.03$ ).

578

579 **Fimbria.**

580 **Day 5.** There was a significant effect of the fimbria volume on the AWN ( $F(1,17)=17.8$ ,  $p=0.0006$ ), as  
581 well as a significant interaction between the volume, genotype, and sex ( $F(2,17)=6.0$ ,  $p=0.01$ ). The  
582 effect was significant in females ( $F(1,7)=10.7$ ,  $p=0.01$ ), as well as for the interaction for fimbria volume  
583 by genotype ( $F(2,7)=5.0$ ,  $p<0.05$ ). There was a trend for slopes differences for APOE3 and APOE4 mice  
584 ( $t$  ratio=2.4,  $p=0.07$ ). These differences were significant between groups of females for APOE2 versus  
585 APOE4 mice ( $t$  ratios=2.8,  $p=0.03$ ), and for APOE3 and APOE4 female mice ( $t$  ratio=3.5,  $p=0.008$ ).  
586 Differences were significant between female and male APOE3 mice ( $t$  ratio=2.7,  $p=0.01$ ), and  
587 showed a trend between female and male APOE4 mice ( $t$  ratio=-2,  $p=0.07$ ). The slopes were different than  
588 0 for APOE4 mice ( $t$  ratio=-3.2,  $p=0.006$ ), and in particular for APOE4 females ( $t$  ratio=-3.7,  $p=0.002$ ), and  
589 showed a trend for APOE3 females ( $t$  ratio=2.1,  $p=0.05$ ), and males ( $t$  ratio=-1.9,  $p=0.08$ ).

590 The FA interaction with genotype was significant ( $F(2,17)=5.1$ ,  $p=0.04$ ). There was a trend for slopes  
591 for APOE3 ( $t$  ratio=-1.6,  $p=0.1$ ) and APOE4 mice ( $t$  ratio=1.6,  $p=0.1$ ), and for slope differences between APOE3  
592 and APOE4 females ( $t$  ratio=-2.2,  $p=0.1$ ).

593 For the degree of connectivity we only found a trend between females and males with APOE3  
594 genotypes ( $t$  ratio=1.7,  $p=0.1$ ). The clustering coefficient interaction by sex also showed a trend ( $t$  ratio=3.2,  
595  $p=0.09$ ).

596 **Day 8.** There was a significant difference between the slopes for volume and AWS between APOE3  
597 and APOE4 mice ( $t$  ratio=-2.6,  $p=0.04$ ).

598 For the degree of connectivity there was a significant interaction with sex ( $F(1,17)=6.3$ ,  $p=0.02$ ), and  
599 there were significant differences between males and females of APOE2 ( $t$  ratio=2.4,  $p=0.03$ ); and a  
600 trend for APOE4 ( $t$  ratio=2.1,  $p=0.05$ ).

601 There was a significant effect of the clustering coefficient ( $F(1,17)=5.8$ ,  $p=0.03$ ).

602

### 603 **Fornix**

604 **Day 5.** There was a trend for the volume as a predictor of AWN for females APOE3 versus APOE4,  $t$   
605 =2.5,  $p=0.06$ ), and for female versus male APOE4 carriers ( $t$  ratio=-1.7,  $p=0.1$ ), and this was similar with  
606 the degree of connectivity for APOE4 females versus males ( $t$  ratio=-1.9,  $p=0.08$ ).

607 **Day 8.** There was a significant effect for the fornix volume ( $F(1,17)=10.6$ ,  $p=0.005$ ), and a trend for the  
608 interaction of fx volume by genotype  $F(2,17)=2.5$ ,  $p=0.1$ . This was significant in males ( $F(1,10)=22.0$ ,  
609  $p=0.001$ ). The slopes were different between APOE2 and APOE3 female mice ( $t$  ratio=-2.7,  $p=0.04$ )  
610 and there was a trend between APOE2 and APOE4 mice ( $t$  ratio=-2.5,  $p=0.06$ ).

611 There was a significant effect for fx FA ( $F(1,17)=5.4$ ,  $p=0.04$ , with a trend for APOE3 females ( $p=0.1$ ).

612 There was a significant effect for the degree of connectivity  $F(2,17)=24.3$ ,  $p=1.1*10^{-5}$ ), and this was  
613 significant within females ( $F(1,7)=6.3$ ,  $p=0.04$ ). The clustering coefficient was also significant  
614 ( $F(1,17)=4.9$ ,  $p=0.04$ ). This was significant within females ( $F(1,7)=6.5$ ,  $p=0.04$ ), with a trend for APOE3  
615 females ( $p=0.1$ ).

616

### 617 **Internal Capsule**

618 **Day 5.** There was a significant interaction of the volume by genotype ( $F(2,17)=3.7$ ,  $p=0.04$ ) and a trend  
619 for the slope differences between APOE3 and APOE4 females ( $t$  ratio=2.2,  $p=0.1$ ).

620 There was a significant effect of FA ( $F(1,17)=7.8$ ,  $p=0.01$ ). There was a trend for the clustering  
621 coefficient slope differences between APOE4 females and males ( $t=1.7$ ,  $p=0.1$ ).

622 **Day8.** There was a significant effect of the FA ( $F(1,17)=12.6$ ,  $p=0.002$ ), with a trend within females  
623 ( $F(1,7)=5.2$ ,  $p=0.06$ ). There was a significant effect of the degree of connectivity within males  
624 ( $F(1,10)=7.3$ ,  $p=0.02$ ).

625

626 **Cerebellar White Matter**

627 **Day 5.** We found no effects of the cerebellum white matter on the winding number at day 5.

628 **Day8.** There was an effect of the clustering coefficient  $F(1,17)=6.1$ ,  $p=0.02$ ), with a trend for differences  
629 between APOE2 and APOE3 ( $t =-2.3$ ,  $p=0.1$ ), and APOE2 and APOE4 ( $t =-2.5$ ,  $p=0.06$ )

630

631

632

Day5

Region	Metric	Within	Comparison	t ratio	p
fi	Volume	F	E2E4	2.843	0.029*
fi	Volume	F	E3E4	3.456	0.008*
fx	FA	F	E3E4	-3.178	0.014*
fx	DEG	F	E3E4	2.903	0.026*
Hc	DEG	F	E3E4	2.109	0.110
fx	Volume	F	E3E4	2.471	0.060
fx	CLUS	F	E3E4	2.393	0.070
ic	Volume	F	E3E4	2.212	0.098
fi	Volume	M/F	E3E4	2.37	0.073

Day5

Region	Metric	Within	Comparison	t ratio	p
fi	Volume	E3	M/F	2.74	0.014*
Hc	DEG	E3	M/F	2.071	0.054
Hc	CLUS	E3	M/F	1.795	0.090
CPu	CLUS	E3	M/F	1.732	0.101
fi	DEG	E3	M/F	1.736	0.101
fi	Volume	E4	M/F	-1.952	0.068
fx	DEG	E4	M/F	-1.896	0.075
fx	CLUS	E4	M/F	-1.628	0.122

Day8

Region	Within	Comparison	t ratio	p	
fi	Volume	M	E3E4	-2.621	0.048*
fx	Volume	F	E2E3	-2.666	0.041*
Hc	Volume	F	E2E3	2.291	0.084
fx	Volume	F	E2E4	-2.487	0.058
ic	Volume	F	E2E4	-2.26	0.089
Hc	DEG	M/F	E2E3	2.216	0.097
Hc	Volume	M/F	E2E3	2.392	0.070
cbw	CLUS	F	E2E3	-2.475	0.060
cbw	CLUS	F	E2E4	-2.253	0.091

Day8

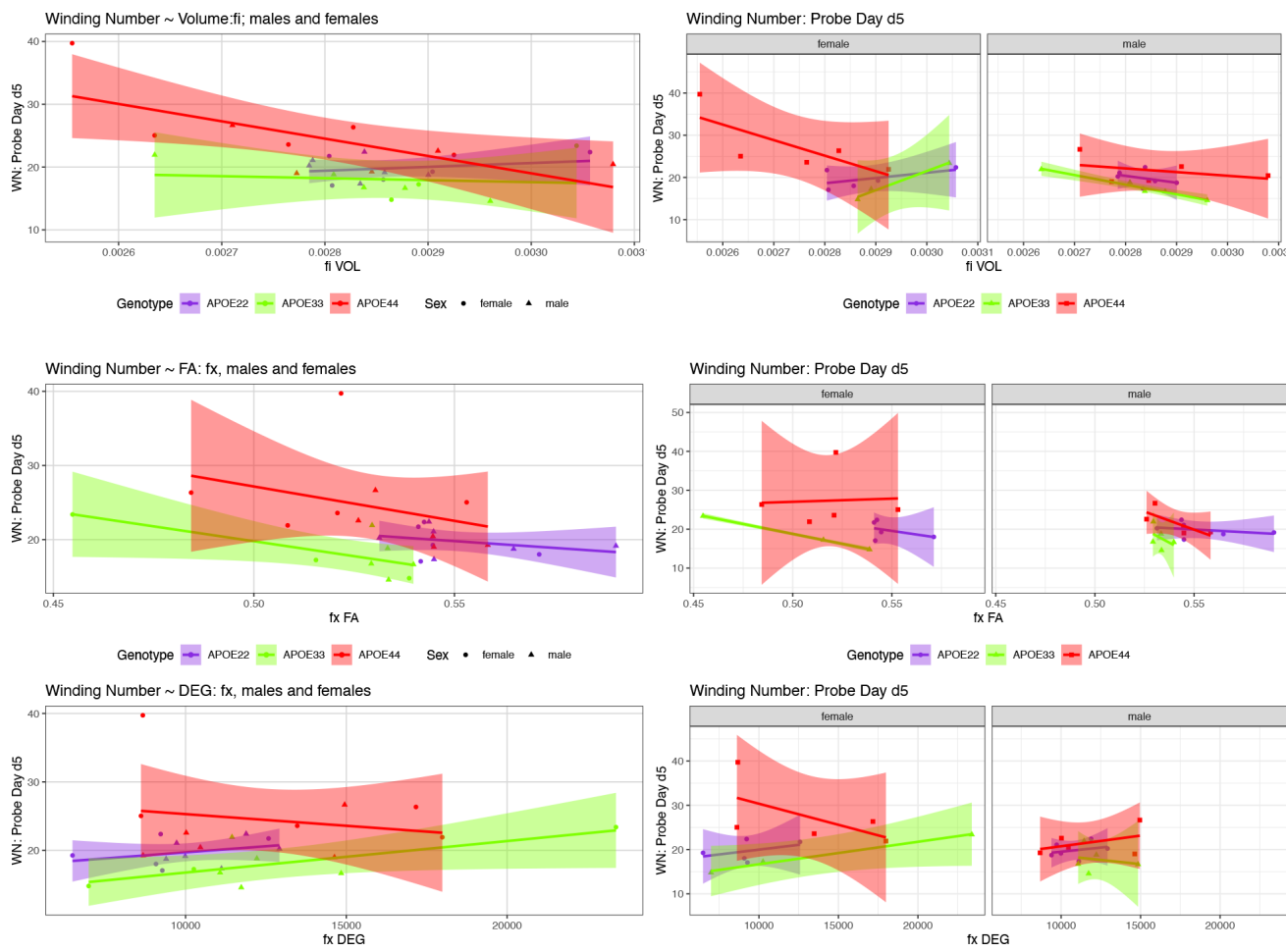
Region	Within	Comparison	t ratio	p	
fi	DEG	E2	M/F	2.435	0.026*
CPu	Volume	E3	M/F	2.343	0.032*
CPu	DEG	E3	M/F	2.198	0.042*
fi	Volume	E3	M/F	2.462	0.025*
Hc	FA	E2	M/F	-1.968	0.066
CPu	Volume	E2	M/F	1.874	0.078
CPu	DEG	E2	M/F	1.724	0.103
fi	FA	E2	M/F	-2.049	0.056
fi	CLUS	E2	M/F	1.65	0.117
ic	DEG	E2	M/F	1.625	0.123
ic	CLUS	E2	M/F	1.775	0.094
cbw	Volume	E2	M/F	-1.748	0.099
Hc	DEG	E3	M/F	2.432	0.026
Hc	CLUS	E3	M/F	1.754	0.097
CPu	FA	E3	M/F	-1.972	0.065
fi	DEG	E3	M/F	2.109	0.050
fi	CLUS	E3	M/F	1.736	0.101
fx	Volume	E3	M/F	1.669	0.113
Hc	FA	E4	M/F	-1.869	0.079

633 **Table 4. Summary of AWN~MRI metrics comparisons.** APOE22: E2, APOE33: E3, APOE44: E4; 634 F: female; M: male.

635

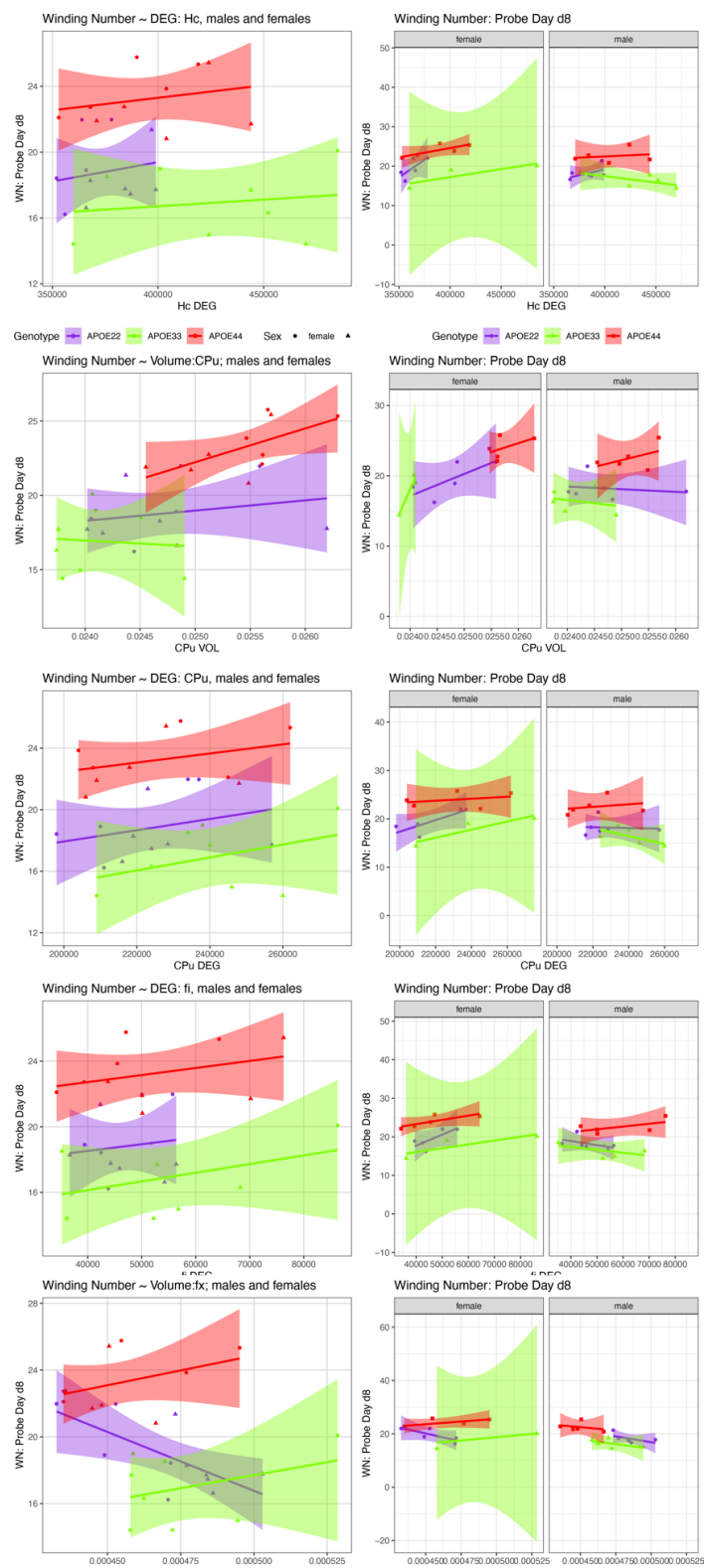
636 Our comparison of the models' slopes revealed differences between groups of females with different  
 637 APOE carriage, both at day 5 (**Figure 7**), and day 8 (**Figure 8**), emphasizing the role of the fornix and  
 638 fimbria, and suggesting that these major players may interact with other brain regions forming more  
 639 complex network that determine spatial navigation. Sex differences were also noted, including in the  
 640 control genotype APOE3 in these circuits, suggesting possible sex modulation of genetic risk for AD.

641



642  
 643

644 **Figure 7. The day 5 AWN~ MRI metrics models.** Slopes were different for the fornix volume between  
 645 APOE2 and APOE4 females ( $p=0.03$ ), and APOE3 versus APOE4 females ( $p=0.008$ ), and there was  
 646 a trend for APOE3 versus APOE4 slopes ( $p=0.07$ ). There was also a significant difference in slopes  
 647 between males and females with APOE3 genotype ( $p=0.01$ ). There were also significant differences  
 648 between APOE3 and APOE4 females in the slopes for fornix FA ( $p=0.01$ ), and degree of connectivity  
 649 ( $p=0.03$ ). There was also a trend for the slope differences between APOE3 and APOE4 females for  
 650 the internal capsule volume ( $p=0.1$ , not shown).



651

652 **Figure 8. The day 8 AWN~ MRI metrics models.** APOE3 mice showed differences between males  
 653 and females in the slopes for the hippocampus degree of connectivity, caudate putamen volume, and  
 654 degree of connectivity, while males and female APOE2 mice were different for the fimbria degree of  
 655 connectivity. The fornix volume showed differences between females APOE2 and APOE3 ( $p=0.04$ ),  
 656 and there was a trend for APOE2 versus APOE4 differences ( $p=0.06$ ).

657

658 **4 Discussion**

659

660 The major known genetic risk for sporadic, or late onset AD is linked to the APOE gene, and it is  
661 conferred by the presence of APOE4 allele. Studying human subjects, or animal models with APOE4  
662 carriage is thus an important strategy for discovering early biomarkers predictive of abnormal aging.  
663 However, in cognitively normal subjects, APOE4 is not always associated with an increased risk of  
664 cognitive deterioration, suggesting that APOE4 effects on structural and/or clinical progression only  
665 become evident in mild cognitive impairment (MCI) and AD (Haller et al. 2017). Still, several studies  
666 have shown spatial navigation/orientation deficits in AD, and some indicated that these changes are  
667 present in MCI patients and even in cognitively healthy APOE4 carriers (Coughlan et al. 2018). It is  
668 important to answer the question whether APOE4 carriers at risk for AD perform spatial navigation  
669 tasks differently from APOE2 and APOE3 carriers. If true, spatial navigation and orientation might  
670 provide novel cognitive evaluation metrics for prodromal or incipient AD, as sensitive and specific  
671 markers of the disease (Coughlan et al. 2018). Rodents provide tools to model AD at prodromal stages,  
672 and test novel interventions to remove pathologies, and slow cognitive decline; thus we were motivated  
673 to explore spatial learning, memory and navigation strategies in mouse models with different genetic  
674 risk for AD.

675 Our premise lies in knowing that humans and also rodents use preferentially one of two navigational  
676 strategies. A spatial strategy (Packard, Hirsh, and White 1989; Iaria et al. 2003) relies on forming  
677 relationships between landmarks in the environment and orienting oneself in relation to those  
678 landmarks. This process requires the ability to form cognitive maps of the environment and the flexibility  
679 to derive a direct path to a target during navigation. The spatial strategy is subserved by the  
680 hippocampus (Morris et al. 1982). In contrast, a response strategy involves learning a series of  
681 stimulus-response associations, e.g. the pattern of left and right turns from a given starting position.  
682 This strategy relies on the caudate putamen, and is inflexible, in that it does not require generating a  
683 de novo, direct path to a target location (Packard, Hirsh, and White 1989) during navigation.

684 The most popular method to assess spatial learning and memory in rodents is the MWM, and several  
685 adaptations of this test have been proposed and adopted in human research. The memory and learning  
686 processes are usually characterized by distance and time measures to a hidden platform, or the  
687 distance and time spent in the target quadrant during learning trials, or probe tests. Few publications  
688 have characterized the swim patterns, and this was usually done by assigning the swim path, according  
689 to its shape (Brody and Holtzman 2006), (Brabazon et al. 2017), (Zhao et al. 2012), into a small number  
690 of discrete categories: direct, chaining, scanning, etc. (Janus 2004). The proportions of time, or  
691 distance spent in each of these categories was then compared.

692 In this work we have introduced a new metric, the AWN, to the battery of tests and metrics used for  
693 assessing the cognition of mouse models of neurological conditions, such as AD. This provides a  
694 quantitative way to describe the continuous curve that is the swim trajectory, during goal directed spatial  
695 navigation. Our analyses showed that this metric is robust to noise, and can be used to compare and  
696 better separate relatively small groups of mice, based on their spatial navigation strategies. The AWN  
697 was sensitive to genotype and sex, discriminating APOE3 mice as having simpler trajectories during  
698 the learning process relative to APOE2 and APOE4 mice, and this effect was strongest in females. The  
699 probe trials revealed that APOE4 mice had more complex, loopier trajectories during memory tests.

700 We have examined whether differences in memory, and spatial navigation strategies were  
701 accompanied by imaging and connectivity changes, and how these metrics were related to the AWN.  
702 This is because proper memory function requires structural and functional connections of networks  
703 (Linden 2007; Piccoli et al. 2015), e.g. involving the dorsal hippocampus (Hc) for spatial memory, and

704 the ventral hippocampus (Hc) for emotional memory (Fanselow and Dong 2010b; Fanselow and Dong  
705 2010a). In rodents, the dorsal Hc and subiculum form a critical network with the anterior cingulate, that  
706 mediates processes such as learning, memory, and navigation.

707 Our results showed that mouse models representing different levels of genetic risk for Alzheimer's  
708 disease performed differently in the spatial memory tests, as assessed with the Morris Water Maze.  
709 We added to the existing body of knowledge the observation that swim paths differ with genotypes not  
710 just in length but also in shape. We introduced a new metric through the absolute winding number,  
711 which gives insight into spatial navigation strategy differences, is robust to noise, and showed  
712 differences between females. Moreover, the absolute winding number discriminated APOE3 carriers  
713 during learning trials, as they have simpler trajectories relative to APOE2 and APOE4 carriers, which  
714 are more similar, and these differences are due to females. During probe trials administered at 1 hour  
715 after the end of learning, the absolute winding number discriminated APOE4 mice relative to APOE2  
716 and APOE3 carriers, as these two groups had more similarly shaped trajectories. Our data on the  
717 spatial search strategy tested three days after the end of the learning trials suggest a genotype "dose"  
718 dependent effect, and this was particularly apparent in females, while APOE4 males were differentiated  
719 relative to APOE2 and APOE3 males, that had more similar search strategies.

720 These behavioral changes were accompanied by differences in the volume of the caudate putamen,  
721 but not the hippocampus. We did however find significant changes in the hippocampal FA, its degree  
722 of connectivity, and clustering coefficient. These underline the roles of hippocampal microstructural  
723 properties and connectivity, and suggest such changes may precede overt neurodegeneration, i.e.  
724 atrophy. The hippocampal degree of connectivity and clustering coefficient did discriminate between  
725 APOE2 and APOE3 mice. The degree of connectivity was also different between APOE2 and APOE4  
726 mice.

727 Besides the hippocampus, microstructural changes were found in the caudate putamen and fornix, and  
728 there was a trend for the internal capsule. Changes in the degree of connectivity were found for the  
729 hippocampus and internal capsule, with a trend for the cerebellar white matter. The clustering  
730 coefficient was different for the hippocampus, and showed a trend for the fornix, internal capsule, and  
731 cerebellar white matter. The clustering coefficient for the hippocampus differentiated APOE2 versus  
732 APOE3 mice, and there was a trend for the fornix, internal capsule, and cerebellar white matter. These  
733 results suggest that carriage of different APOE alleles results in different connectivity for regions  
734 involved in circuits related to spatial navigation, learning and memory, as well as the associated motor  
735 task execution. Together, our results support the importance of the fornix in rodent spatial navigation,  
736 in agreement with evidence from human studies (Hodgetts et al. 2020).

737 As we hypothesized that imaging metrics could help predict changes in the spatial trajectory shape,  
738 the AWN on day 5 found that hippocampal FA, as well as the caudate putamen volume and FA, differed  
739 significantly among the three APOE genotypes. There was an effect of internal capsule FA. We also  
740 found that the slopes of AWN~ fimbria volume were significantly different for APOE3 versus APOE4  
741 females, and for APOE2 versus APOE4 females. Our results denoted that different strategies were  
742 used by APOE4 females. Interestingly the AWS~ internal capsule only had a zero slope for APOE4  
743 mice (data not shown), suggesting these mice may rely more on striatal circuits to accomplish their  
744 goal oriented navigation task.

745 At 3 days after the last learning trial (day 8), we found stronger relationships between the imaging  
746 metrics and the AWN. The hippocampal FA, caudate putamen volume, as well as the fornix volume  
747 were also significant. Importantly, these data support the role of the fornix in determining the shape of  
748 the swim path, or spatial navigation strategy, as all metrics were significant (volume, FA, degree of  
749 connectivity, and clustering coefficient). The internal capsule FA and degree of connectivity were also  
750 significant. Regions for which connectivity was a predictor of the AWN at 3 days after the last learning  
751 trial were the fimbria, fornix, and cerebellum white matter. In summary our data support the role of the

752 fornic in spatial memory and navigation, and demonstrates involvement of other regions, including the  
753 caudate putamen, and cerebellar white matter.

754 Due to our limited sample sizes, and the fact that we only investigated a small set of regions, we were  
755 unable to dissect whole circuits, or the different roles of these structures in different genotypes.  
756 However, our data showed slope differences for the AWN-fimbria model within females: APOE2 vs  
757 APOE4 ( $p= 0.03$ ); and for APOE3 vs APOE4 females ( $p= 0.0080$ ). At day 8 there were slope  
758 differences between males of APOE3 and APOE4 genotypes ( $t=-2.6$ ,  $p<0.05$ ). This suggests that  
759 different circuits, or different contributions of the same circuits in spatial navigation in mice with different  
760 APOE genotypes, and of different sexes. Further studies should investigate the association between  
761 vulnerable brain circuits and cognitive traits, in particular to reveal sex differences.

762 Ours is not a comprehensive study to dissect the role of vulnerable circuits in spatial navigation,  
763 learning and memory. Rather it is proposing a hypothesis, based on a subselection of brain regions  
764 and connections, in particular those involving the hippocampal (allocentric) and striatal (egocentric,  
765 and procedural) based circuits. These circuits are likely to interact in spatial navigation, and our data  
766 suggest that the presence of different APOE alleles plays role (Goodroe, Starnes, and Brown 2018).  
767 This is important in the context of AD related changes in spatial memory, as it may point to specific  
768 pathways (Neuner et al. 2017). The use of this metric in a full brain analysis will likely provide important  
769 new leads in our quest to understand the early changes of APOE-related vulnerability and mechanisms,  
770 and to reveal early biomarkers.

771

752 **Conflict of Interest**

773 *The authors declare that the research was conducted in the absence of any commercial or financial*  
774 *relationships that could be construed as a potential conflict of interest.*

765 **Author Contributions**

776 AB, DL, CAC, and DD conceived the study, devised methods, wrote and edited the manuscript. NB  
777 generated the mouse lines, suggested ideas and analyses, edited the manuscript; and together with  
778 CAC and CLW participated in the interpretation of the behavioral and imaging data. AN, and AB  
779 performed experiments. AB, AN, RJA, JAS, DL performed analyses.

780 **Funding**

781 This work was supported by RF1 AG057895, and R01 AG066184, U24 CA220245, RF1 AG070149,  
782 R01 MH118927, and the Bass Connections program at Duke.

783 **Acknowledgments**

784 This work was supported by RF1 AG057895, and R01 AG066184, U24 CA220245, RF1 AG070149,  
785 R01 MH118927, and the Bass Connections program at Duke. We are grateful to the members of the  
786 Duke Radiology and Duke Neurology Departments for generously sharing advice, support and  
787 resources needed for the experiments, in particular Gary Cofer, Lucy Upchurch, Brian Mace, Viviana  
788 Cantillana, and Joan G Wilson. We are grateful to NIH and the Bass Connections program for  
789 supporting our research.

790 **Data Availability Statement**

791 The datasets analyzed for this study can be obtained from the first authors. Code is shared at  
792 <https://github.com/AD-Decode/awn>.

793 **Contribution to the Field**

794 We studied animals modeling genetic risk for late onset Alzheimer's disease using behavior and MR  
795 imaging. We introduce a new metric, the absolute winding number, to characterize the spatial search  
796 strategy, through the shape of the swim path. The absolute winding number better differentiated  
797 APOE3 carriers, through their straighter swim paths relative to APOE2 and APOE4 genotypes. This  
798 novel metric was sensitive to sex differences, supporting increased vulnerability in APOE4 females.  
799 We hypothesized differences in spatial memory and navigation strategies are linked to differences in  
800 brain networks, and showed that different genotypes have different reliance on the hippocampal and  
801 caudate putamen circuits, pointing to a role for white matter connections. Our results support a  
802 departure from a hippocampal centric to a brain network approach, and open new avenues for  
803 identifying regions linked to increased risk for AD, before overt disease manifestation. Further  
804 exploration of novel biomarkers based on spatial navigation strategies may enlarge the windows of  
805 opportunity for interventions. The proposed framework will be significant in dissecting vulnerable  
806 circuits associated with cognitive changes in prodromal Alzheimer's disease.

807

808 **Tables and Figure Legends**

809 **Table1.** Animal groups distribution by genotype, sex, and age range.

810 **Table 2. APOE genotype differences in MRI metrics i.e. volume, fractional anisotropy (FA),**

811 **degree of connectivity (DEG), and clustering coefficient (CLUS)** for regions of interest including:

812 hippocampus (Hc), caudate putamen (CPu), fimbria (fi), fornix (fx), internal capsul (ic), and cerebellar

813 white matter (cbw).

814 **Table 3. Main ANOVA results on the linear models predicting AWN based on MRI metrics.**

815 **Table 4. Summary of AWN~MRI metrics comparisons.** APOE22: E2, APOE33: E3, APOE44: E4;

816 F: female; M: male.

817 **Figure 1. Examples of swim paths shapes for animals with APOE2, APOE3, and APOE4**

818 **genotypes.** Qualitative observations suggest that swim paths differed not just in length, but also in

819 shape. Trajectories are presented for the last trial in day 1 (A), probe in day 5 (B) and probe in day 8

820 (C). We chose animals illustrating medium (APOE2: learning=22, d5=17.3; d8=16.6), medium-small

821 (APOE3: learning=13, d5=16.8, d8=15), and large winding numbers (APOE4: learning=26, d5=39;

822 d8=23). APOE22: homozygous for APOE2; APOE33: homozygous for APOE3; APOE44: homozygous

823 for APOE4.

824 **Figure 2. Learning trials.** Mice swam shorter distances over the 5 testing days until reaching the

825 hidden platform, indicating that they were learning. Meanwhile, the percentage time swam in the target

826 quadrant increased with time. The absolute winding number clearly discriminated the APOE3 mice

827 relative to APOE2 and APOE4 carriers, which used more similarly shaped trajectories. The effects

828 were larger in females across the 5 days. F: female; M: male. Graphs show mean±standard error.

829 **Figure 3. Probe trials 1 hour after ending the learning trials.** Long term memory tested one hour

830 after the end of learning trials indicated that APOE4 mice swam less than APOE2 and APOE3 mice,

831 and the data suggested a “dose dependent” genotype effect in males. APOE3 mice spent most of their

832 swimming in the target quadrant (~80%), while APOE2 and APOE4 mice spent (~50%) of their

833 swimming in the target quadrant, but the differences between males and females were not significant.

834 APOE2 and APOE4 mice were more similar, while significant differences were noticed between

835 APOE2 and APOE3 mice, as well as between APOE3 and APOE4 female mice. The shape of the swim

836 path, described by the absolute winding number showed similarities between APOE2 and APOE3

837 mice, but higher loopiness for APOE4 mice. These differences were largest for females. F: female; M:

838 male. Graphs show mean±standard error.

839 **Figure 4. Probe trials 3 days after ending the learning trials (mean±standard error).** A. The largest

840 effects in terms of total distance were seen in males, where APOE4 mice swam the shortest distances.

841 Our analysis does not capture stops when animals may orient themselves. B. The percentage time

842 swam in the target quadrant was largest in APOE3 mice relative to APOE2 and APOE4 mice. This

843 effect was driven largely by females, while male mice with APOE2 genotype spent less time in the

844 target quadrant relative to other mice, and APOE3 and APOE4 mice performed similarly. A dose

845 dependent effect was apparent in the absolute winding number for all genotypes, and this was reflected

846 mostly in females. Male mice with APOE2 and APOE3 genotypes used similar strategies, females with

847 APOE2 genotypes having smaller winding numbers. APOE4 males had loopier swim trajectories

848 relative to both APOE2 and APOE3 mice, which had similar trajectories. F: female; M: male. Graphs

849 show mean±standard error.

850 **Figure 5. Regions of interest for spatial navigation and their MRI associated metrics.** We

851 segmented selected brain regions involved in spatial navigation, including the hippocampus (Hc),

852 caudate putamen (CPu), and their major connections (fimbria: fi, and fornix: fx; and internal capsule :  
853 ic, respectively), to which we added the cerebellar white matter, and we have measured their volumes  
854 (A). These regions were characterized by diffusion based measurements, which characterize  
855 microstructure through texture, and may vary along tracts (such as fractional anisotropy) (B). Finally  
856 we characterized their connectivity with other brain regions (C). Abbreviations and region indices  
857 correspond to the CHASS atlas (Calabrese et al. 2015),(Anderson et al. 2019) and Paxinos mouse  
858 brain atlas: Hc: hippocampus; CPu: caudate putamen, fi: fimbria, fx: fornix, ic: internal capsule, cbw:  
859 cerebellar white matter.

860 **Figure 6. Imaging and network markers for volume, FA, degree of connectivity and clustering**  
861 **coefficient showed APOE genotype differences.**

862 **Figure 7. The day 5 AWN~ MRI metrics models.** Slopes were different for the fimbria volume between  
863 APOE2 and APOE4 females ( $p=0.03$ ), and APOE3 versus APOE4 females ( $p=0.008$ ), and there was  
864 a trend for APOE3 versus APOE4 slopes ( $p=0.07$ ). There was also a significant difference in slopes  
865 between males and females with APOE3 genotype ( $p=0.01$ ). There were also significant differences  
866 between APOE3 and APOE4 females in the slopes for fornix FA ( $p=0.01$ ), and degree of connectivity  
867 ( $p=0.03$ ). There was also a trend for the slope differences between APOE3 and APOE4 females for  
868 the internal capsule volume ( $p=0.1$ , not shown).

869 **Figure 8. The day 8 AWN~ MRI metrics models.** APOE3 mice showed differences between males  
870 and females in the slopes for the hippocampus degree of connectivity, caudate putamen volume, and  
871 degree of connectivity, while males and female APOE2 mice were different for the fimbria degree of  
872 connectivity. The fornix volume showed differences between females APOE2 and APOE3 ( $p=0.04$ ),  
873 and there was a trend for APOE2 versus APOE4 differences ( $p=0.06$ ).

874

875

876

877 **REFERENCES**

878 Alzheimer's Association. 2021. 'ALZHEIMER'S DISEASE FACTS AND FIGURES',  
879 <https://www.alz.org/media/Documents/alzheimers-facts-and-figures.pdf>.

880 Anderson, R. J., J. J. Cook, N. Delpratt, J. C. Noul, B. Gu, J. O. McNamara, B. B. Avants, G. A.  
881 Johnson, and A. Badea. 2019. 'Small Animal Multivariate Brain Analysis (SAMBA) - a High  
882 Throughput Pipeline with a Validation Framework', *Neuroinformatics*, 17: 451-72.

883 Babayan, Benedicte M., Aurélie Watilliaux, Guillaume Viejo, Anne-Lise Paradis, Benoît Girard, and  
884 Laure Rondi-Reig. 2017. 'A hippocampo-cerebellar centred network for the learning and  
885 execution of sequence-based navigation', *Scientific Reports*, 7: 17812.

886 Badea, A., W. Wu, J. Shuff, M. Wang, R. J. Anderson, Y. Qi, G. A. Johnson, J. G. Wilson, S. Koudoro,  
887 E. Garyfallidis, C. A. Colton, and D. B. Dunson. 2019. 'Identifying Vulnerable Brain Networks  
888 in Mouse Models of Genetic Risk Factors for Late Onset Alzheimer's Disease', *Front  
889 Neuroinform*, 13: 72.

890 Bermudez-Contreras, Edgar, Benjamin J. Clark, and Aaron Wilber. 2020. 'The Neuroscience of Spatial  
891 Navigation and the Relationship to Artificial Intelligence', *Frontiers in Computational  
892 Neuroscience*, 14.

893 Bohbot, V. D., J. Lerch, B. Thorndycraft, G. Iaria, and A. P. Zijdenbos. 2007a. 'Gray matter differences  
894 correlate with spontaneous strategies in a human virtual navigation task', *J Neurosci*, 27: 10078-  
895 83.

896 Bohbot, Véronique D, Giuseppe Iaria, and Michael Petrides. 2004. 'Hippocampal function and spatial  
897 memory: evidence from functional neuroimaging in healthy participants and performance of  
898 patients with medial temporal lobe resections', *Neuropsychology*, 18: 418.

899 Bohbot, Véronique D., Jason Lerch, Brook Thorndycraft, Giuseppe Iaria, and Alex P. Zijdenbos.  
900 2007b. 'Gray Matter Differences Correlate with Spontaneous Strategies in a Human Virtual  
901 Navigation Task', *The Journal of Neuroscience*, 27: 10078.

902 Brabazon, F., C. M. Wilson, S. Jaiswal, J. Reed, W. H. Nd Frey, and K. R. Byrnes. 2017. 'Intranasal  
903 insulin treatment of an experimental model of moderate traumatic brain injury', *J Cereb Blood  
904 Flow Metab*, 37: 3203-18.

905 Brody, D. L., and D. M. Holtzman. 2006. 'Morris water maze search strategy analysis in PDAPP mice  
906 before and after experimental traumatic brain injury', *Exp Neurol*, 197: 330-40.

907 Calabrese, E., A. Badea, G. Cofer, Y. Qi, and G. A. Johnson. 2015. 'A Diffusion MRI Tractography  
908 Connectome of the Mouse Brain and Comparison with Neuronal Tracer Data', *Cereb Cortex*,  
909 25: 4628-37.

910 Coughlan, Gillian, Antoine Coutrot, Mizzanur Khondoker, A. Minihane, Hugo Spiers, and Michael  
911 Hornberger. 2018. *Impact of Sex and APOE Status on Spatial Navigation in Pre-symptomatic  
912 Alzheimer's disease*.

913 Eichenbaum, H., C. Stewart, and R. G. Morris. 1990. 'Hippocampal representation in place learning', *J  
914 Neurosci*, 10: 3531-42.

915 Fanselow, M. S., and H. W. Dong. 2010a. 'Are the dorsal and ventral hippocampus functionally distinct  
916 structures?', *Neuron*, 65: 7-19.

917 Fanselow, Michael S., and Hong-Wei Dong. 2010b. 'Are the Dorsal and Ventral Hippocampus  
918 Functionally Distinct Structures?', *Neuron*, 65: 7-19.

919 Garyfallidis, Eleftherios, Matthew Brett, Bagrat Amirbekian, Ariel Rokem, Stefan Van Der Walt,  
920 Maxime Descoteaux, and Ian Nimmo-Smith. 2014. 'Dipy, a library for the analysis of diffusion  
921 MRI data', *Front Neuroinform*, 8: 8.

922 Goodroe, Sarah C., Jon Starnes, and Thackery I. Brown. 2018. 'The Complex Nature of Hippocampal-  
923 Striatal Interactions in Spatial Navigation', *Frontiers in Human Neuroscience*, 12: 250.

924 Haller, S., M. L. Montandon, C. Rodriguez, M. Ackermann, F. R. Herrmann, and P. Giannakopoulos.  
925 2017. 'APOE\*E4 Is Associated with Gray Matter Loss in the Posterior Cingulate Cortex in  
926 Healthy Elderly Controls Subsequently Developing Subtle Cognitive Decline', *AJNR. American  
927 journal of neuroradiology*, 38: 1335-42.

928 Hodgetts, C. J., M. Stefani, A. N. Williams, B. S. Kolarik, A. P. Yonelinas, A. D. Ekstrom, A. D.  
929 Lawrence, J. Zhang, and K. S. Graham. 2020. 'The role of the fornix in human navigational  
930 learning', *Cortex*, 124: 97-110.

931 Hort, J., J. Laczó, M. Vyhálek, M. Bojar, J. Bures, and K. Vlcek. 2007. 'Spatial navigation deficit in  
932 amnestic mild cognitive impairment', *Proc Natl Acad Sci U S A*, 104: 4042-7.

933 Iaria, Giuseppe, Michael Petrides, Alain Dagher, Bruce Pike, and Véronique D Bohbot. 2003.  
934 'Cognitive strategies dependent on the hippocampus and caudate nucleus in human navigation:  
935 variability and change with practice', *Journal of Neuroscience*, 23: 5945-52.

936 Janus, C. 2004. 'Search strategies used by APP transgenic mice during navigation in the Morris water  
937 maze', *Learn Mem*, 11: 337-46.

938 Knouff, C., O. Briand, S. Lestavel, V. Clavey, M. Altenburg, and N. Maeda. 2004. 'Defective VLDL  
939 metabolism and severe atherosclerosis in mice expressing human apolipoprotein E isoforms but  
940 lacking the LDL receptor', *Biochim Biophys Acta*, 1684: 8-17.

941 Konishi, Kyoko, Venkat Bhat, Harrison Banner, Judes Poirier, Ridha Joober, and Véronique D.  
942 Bohbot. 2016. 'APOE2 Is Associated with Spatial Navigational Strategies and Increased Gray  
943 Matter in the Hippocampus', *Frontiers in Human Neuroscience*, 10.

944 Linden, D. E. 2007. 'The working memory networks of the human brain', *Neuroscientist*, 13: 257-67.

945 McDonald, Robert J, and Norman M White. 1994. 'Parallel information processing in the water maze:  
946 evidence for independent memory systems involving dorsal striatum and hippocampus',  
947 *Behavioral and neural biology*, 61: 260-70.

948 Michaelson, D. M. 2014. 'APOE ε4: the most prevalent yet understudied risk factor for Alzheimer's  
949 disease', *Alzheimers Dement*, 10: 861-8.

950 Morris, R. G., P. Garrud, J. N. Rawlins, and J. O'Keefe. 1982. 'Place navigation impaired in rats with  
951 hippocampal lesions', *Nature*, 297: 681-3.

952 Neuner, S. M., L. A. Wilmott, B. R. Hoffmann, K. Mozhui, and C. C. Kaczorowski. 2017.  
953 'Hippocampal proteomics defines pathways associated with memory decline and resilience in  
954 normal aging and Alzheimer's disease mouse models', *Behav Brain Res*, 322: 288-98.

955 Novellino, Fabiana, María Eugenia López, Maria Grazia Vaccaro, Yus Miguel, María Luisa Delgado,  
956 and Fernando Maestu. 2019. 'Association Between Hippocampus, Thalamus, and Caudate in  
957 Mild Cognitive Impairment APOEε4 Carriers: A Structural Covariance MRI Study', *Frontiers  
958 in neurology*, 10: 1303-03.

959 Packard, M. G., R. Hirsh, and N. M. White. 1989. 'Differential effects of fornix and caudate nucleus  
960 lesions on two radial maze tasks: evidence for multiple memory systems', *The Journal of  
961 Neuroscience*, 9: 1465.

962 Pennartz, C. M., R. Ito, P. F. Verschure, F. P. Battaglia, and T. W. Robbins. 2011. 'The hippocampal-  
963 striatal axis in learning, prediction and goal-directed behavior', *Trends Neurosci*, 34: 548-59.

964 Piccoli, Tommaso, Giancarlo Valente, David E. J. Linden, Marta Re, Fabrizio Esposito, Alexander T.  
965 Sack, and Francesco Di Salle. 2015. 'The default mode network and the working memory  
966 network are not anti-correlated during all phases of a working memory task', *PLoS one*, 10:  
967 e0123354-e54.

968 Robert Anderson, Nian Wang, James Cook, Gary Cofer, Russell Dibb, G. Johnson, Alexandra  
969 Badea. 2018. "A High Performance Computing Cluster Implementation Of Compressed  
970 Sensing Reconstruction For MR Histology." In *Proc. Intl. Soc. Mag. Reson. Med.*

971 Rochefort, C., J. M. Lefort, and L. Rondi-Reig. 2013. 'The cerebellum: a new key structure in the  
972 navigation system', *Front Neural Circuits*, 7: 35.

973 Rubinov, M., and O. Sporns. 2010. 'Complex network measures of brain connectivity: uses and  
974 interpretations', *NeuroImage*, 52: 1059-69.

975 Stoianov, I. P., C. M. A. Pennartz, C. S. Lansink, and G. Pezzulo. 2018. 'Model-based spatial  
976 navigation in the hippocampus-ventral striatum circuit: A computational analysis', *PLoS  
977 Comput Biol*, 14: e1006316.

978 Sullivan, P. M., H. Mezdour, S. H. Quarfordt, and N. Maeda. 1998. 'Type III hyperlipoproteinemia and  
979 spontaneous atherosclerosis in mice resulting from gene replacement of mouse Apoe with  
980 human Apoe\*2', *J Clin Invest*, 102: 130-5.

981 Tucker, Laura B., Alexander G. Velosky, and Joseph T. McCabe. 2018. 'Applications of the Morris  
982 water maze in translational traumatic brain injury research', *Neuroscience & Biobehavioral  
983 Reviews*, 88: 187-200.

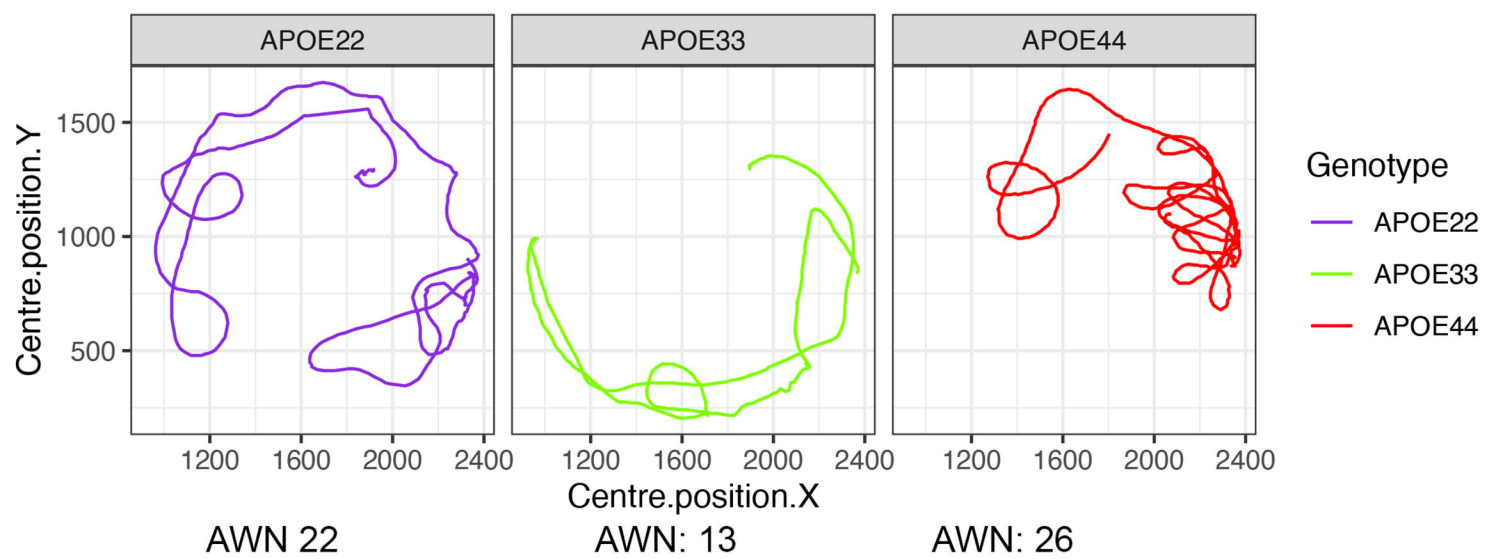
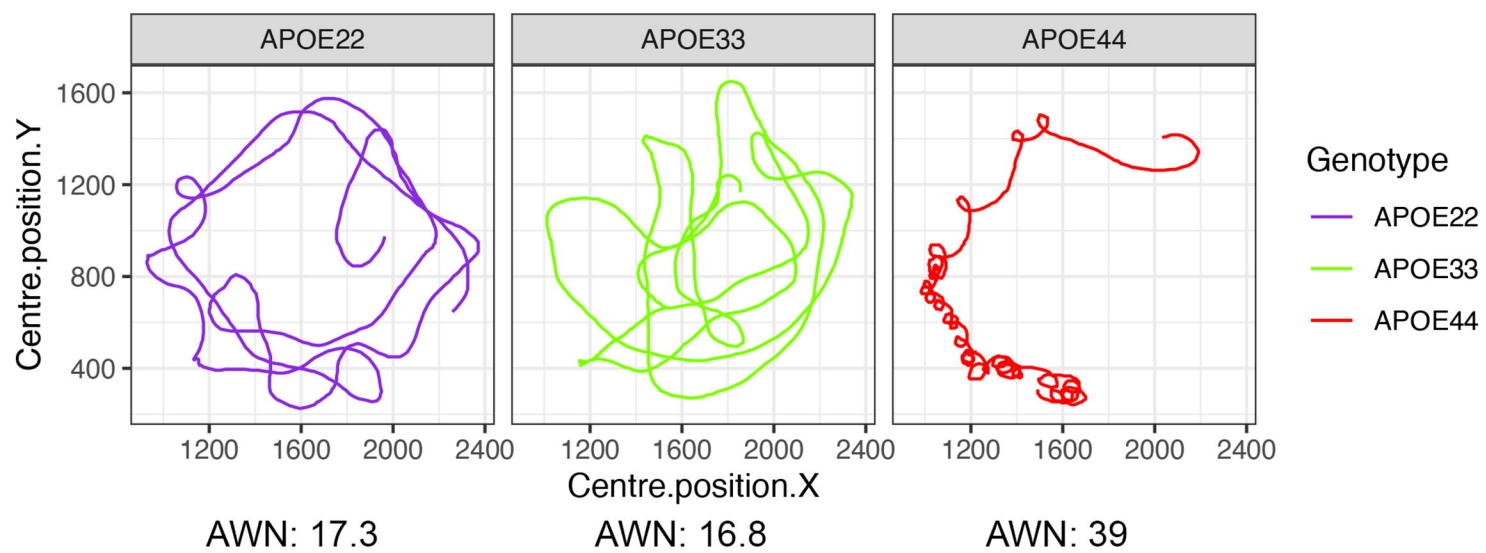
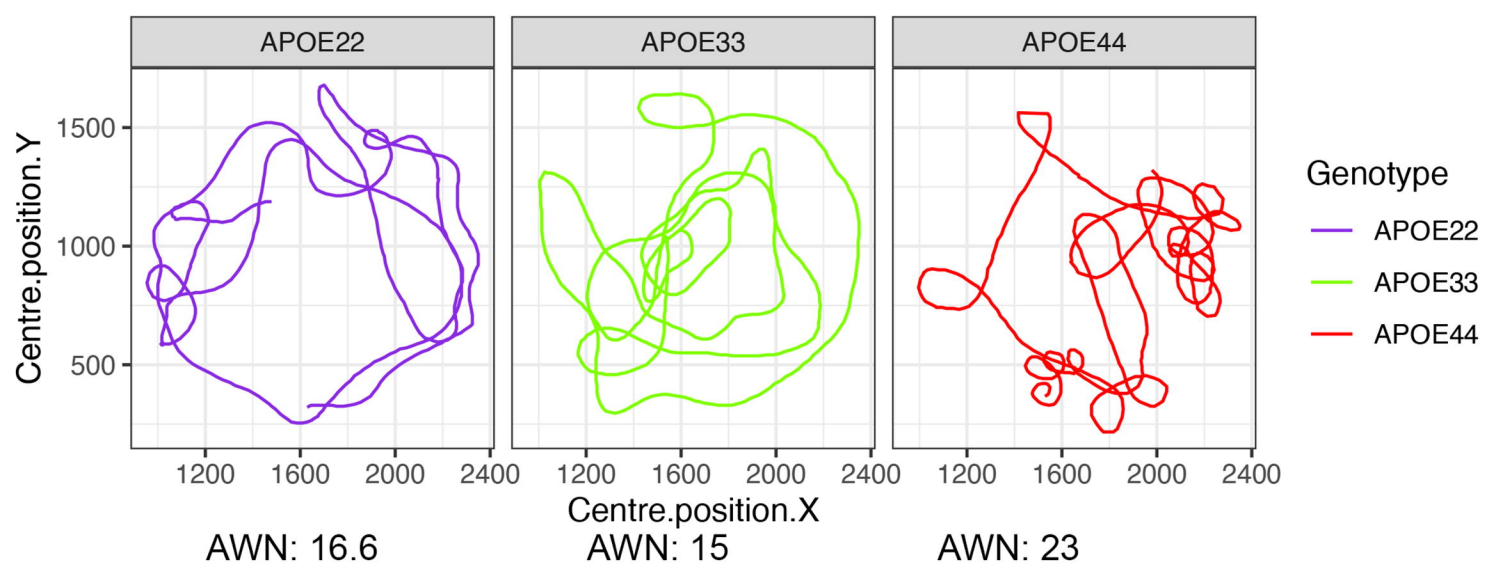
984 Uecker M; Ong F; Tamir JI; Bahri, D; Virtue P, Cheng JY; Zhang T; Lustig M. 2015. "Berkeley  
985 Advanced Reconstruction Toolbox. Annual Meeting ISMRM." In *ISMRM*. Toronto: Proc Intl  
986 Soc Mag Reson Med.

987 Wang, N., R. J. Anderson, A. Badea, G. Cofer, R. Dibb, Y. Qi, and G. A. Johnson. 2018. 'Whole  
988 mouse brain structural connectomics using magnetic resonance histology', *Brain Struct Funct*,  
989 223: 4323-35.

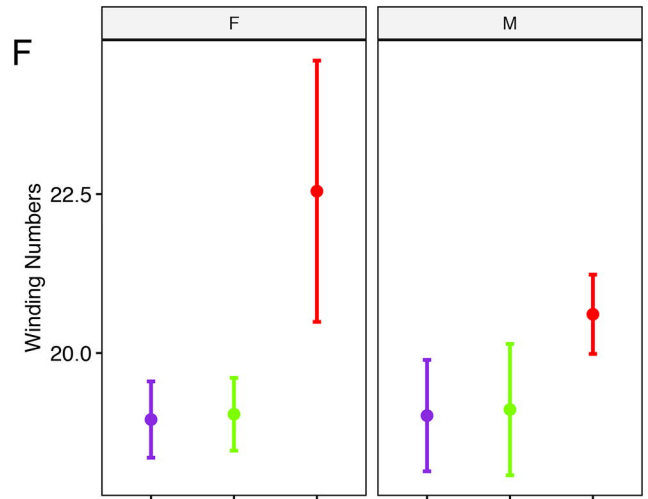
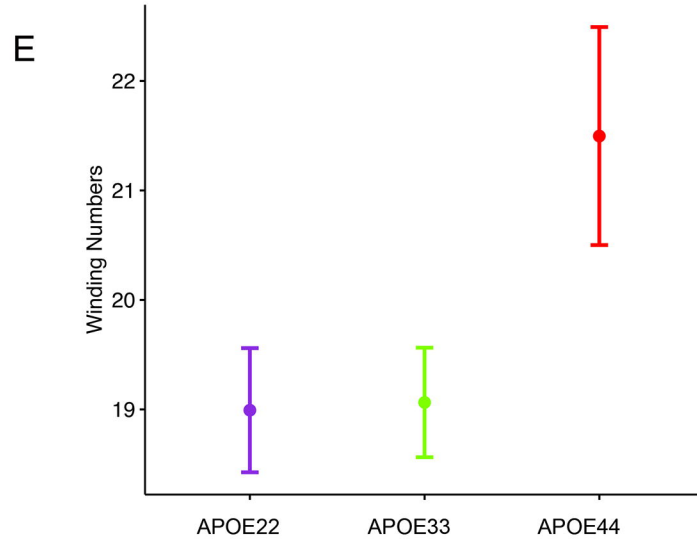
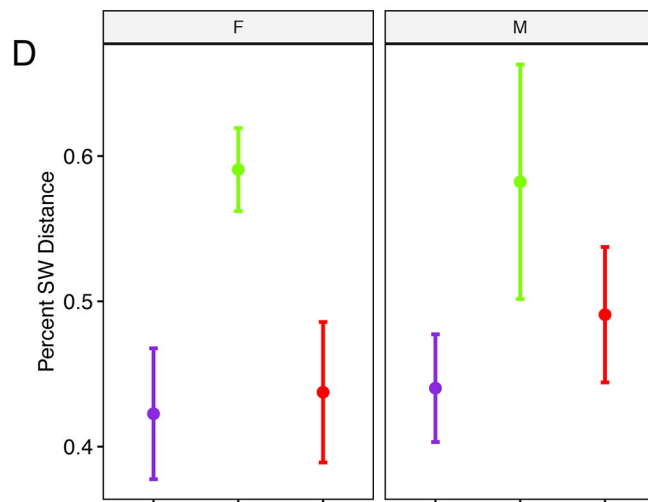
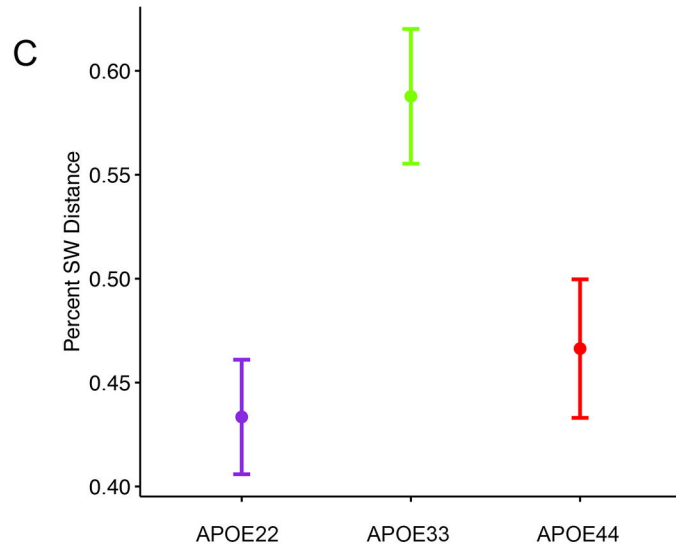
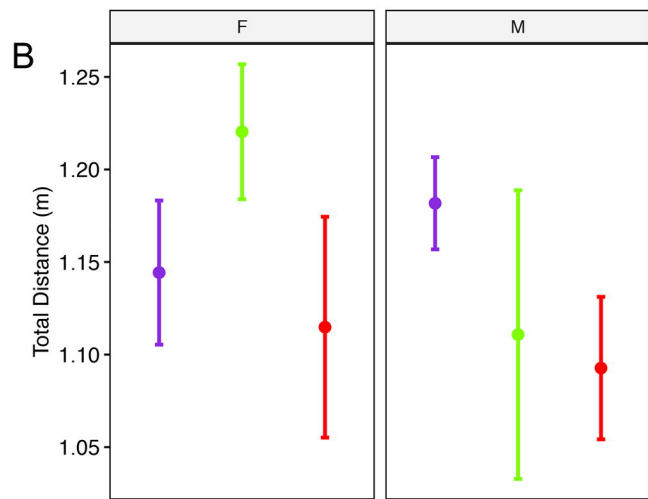
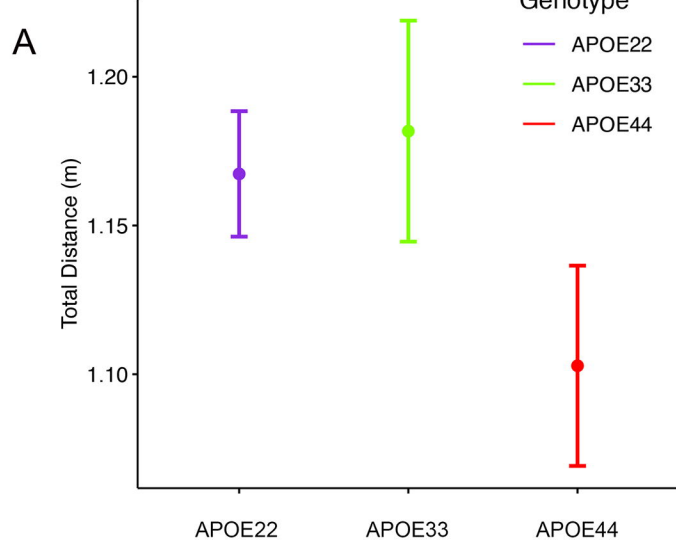
990 Wu, L., and L. Zhao. 2016. 'ApoE2 and Alzheimer's disease: time to take a closer look', *Neural Regen  
991 Res*, 11: 412-3.

992 Zhao, Z., D. J. Loane, M. G. Murray, 2nd, B. A. Stoica, and A. I. Faden. 2012. 'Comparing the  
993 predictive value of multiple cognitive, affective, and motor tasks after rodent traumatic brain  
994 injury', *J Neurotrauma*, 29: 2475-89.

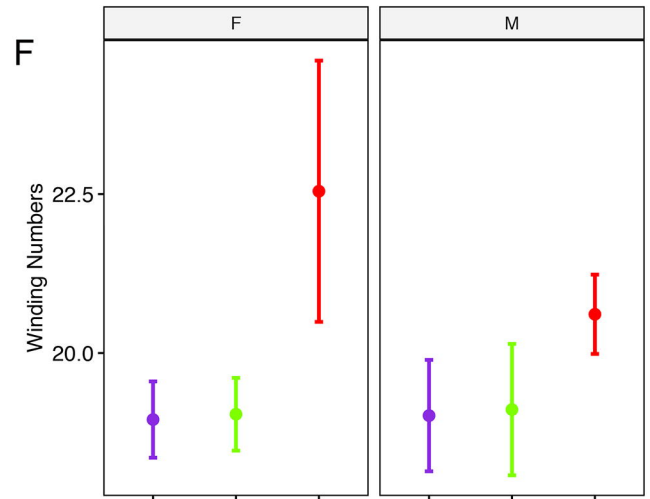
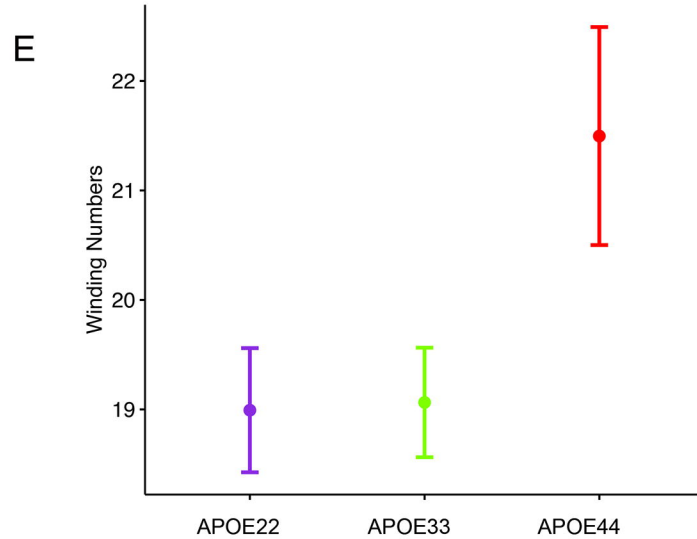
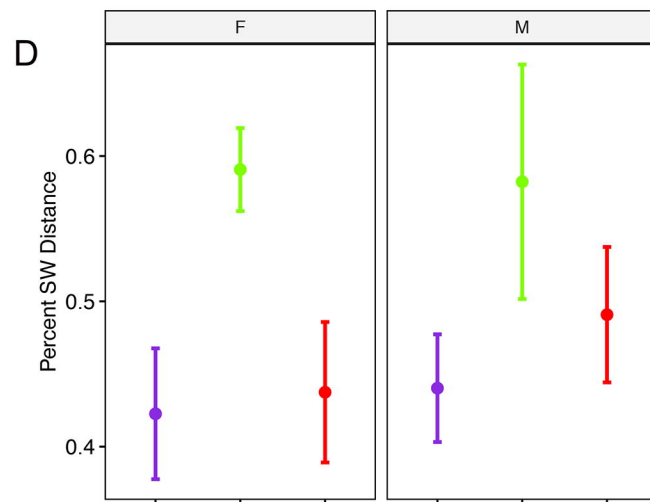
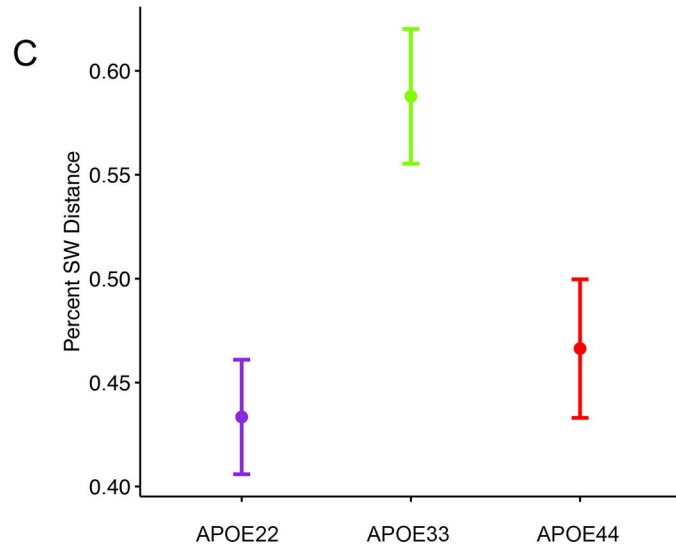
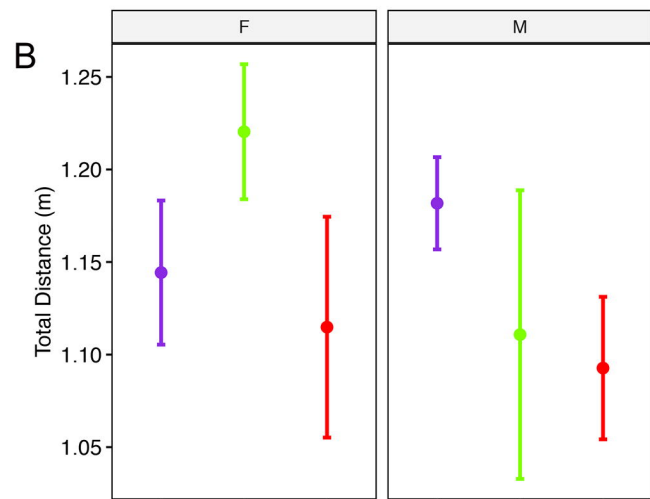
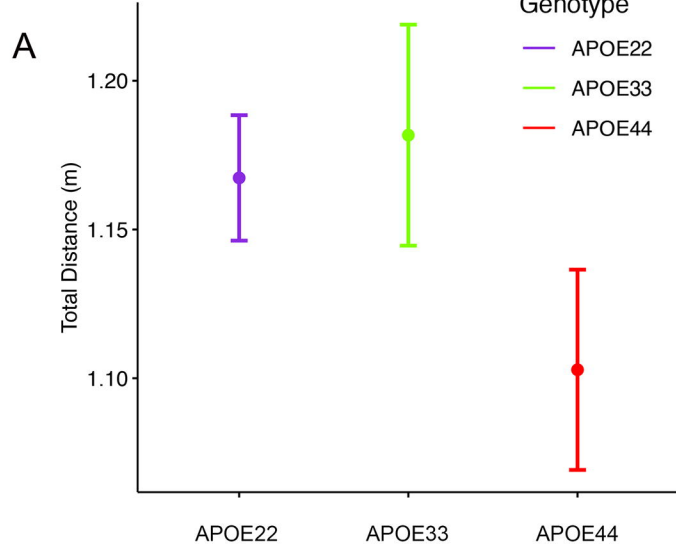
995

**A:Learning Trial 4, Day 1****B:Probe Day 5****C:Probe Day 8**

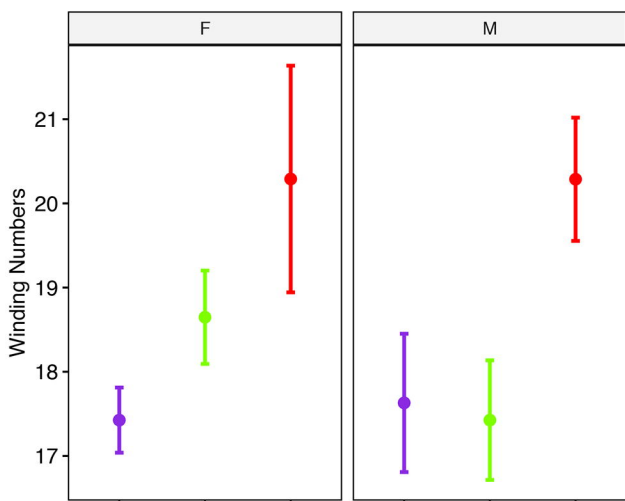
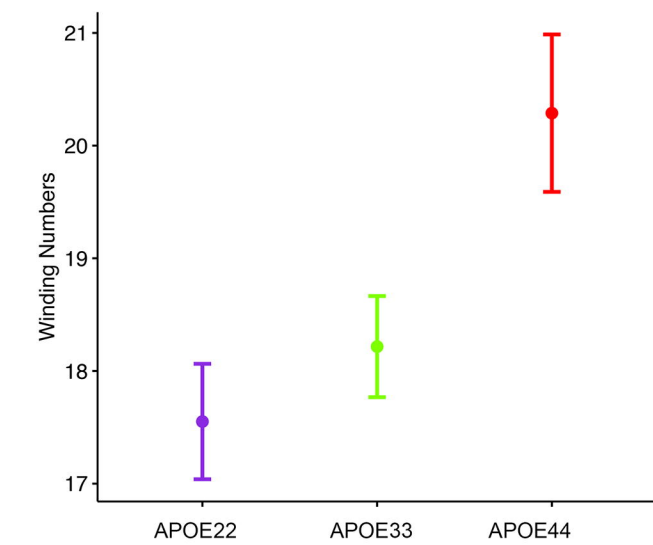
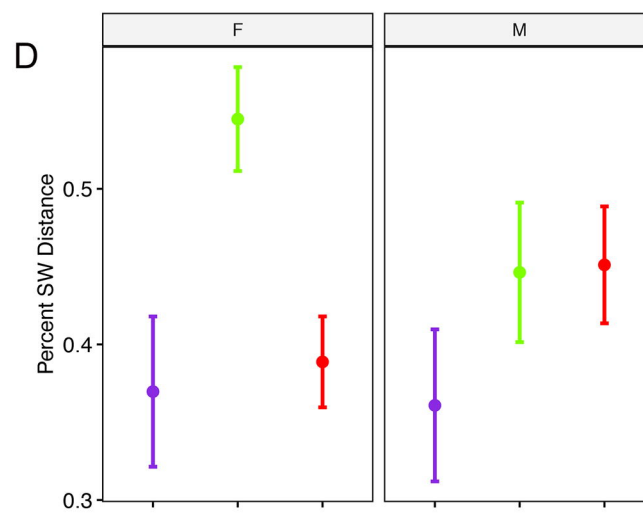
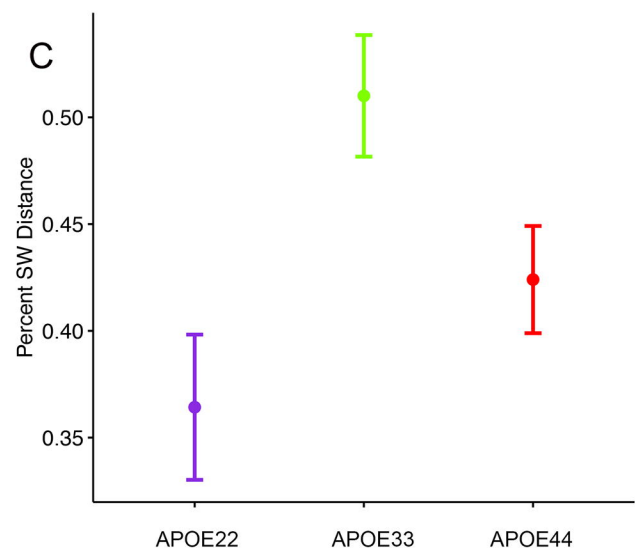
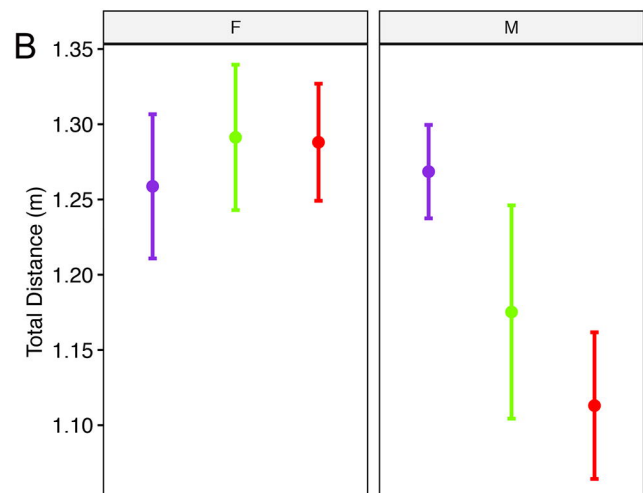
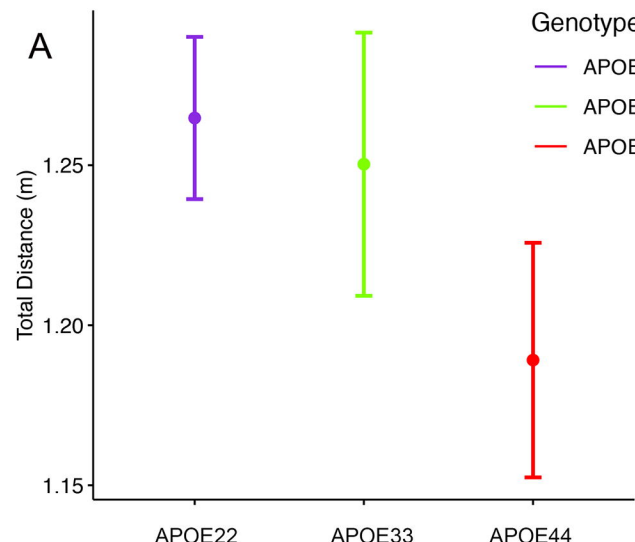
# Probe Day 5



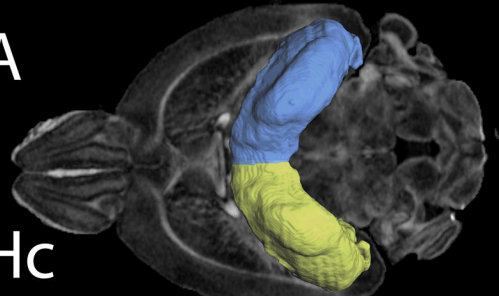
# Probe Day 5



# Probe Day 8

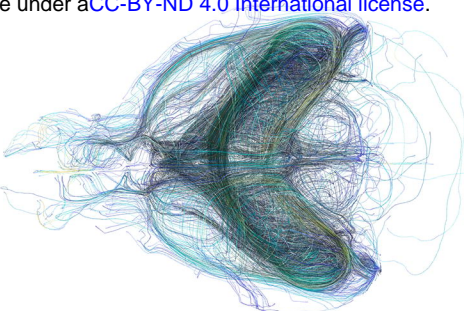


A

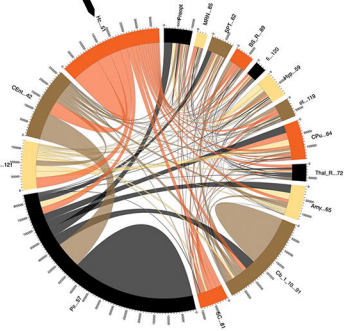


Hc

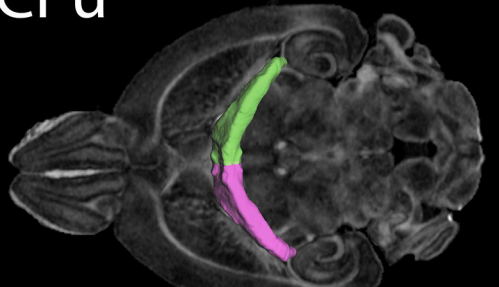
B



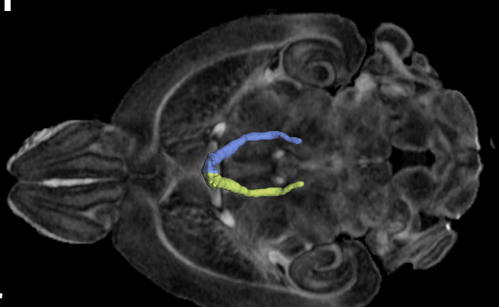
C



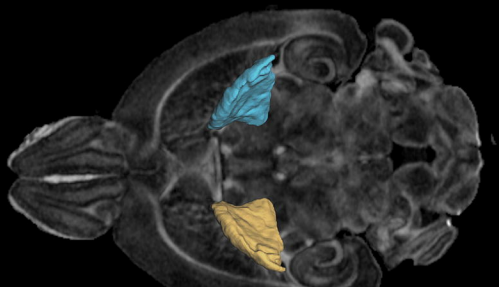
CPy



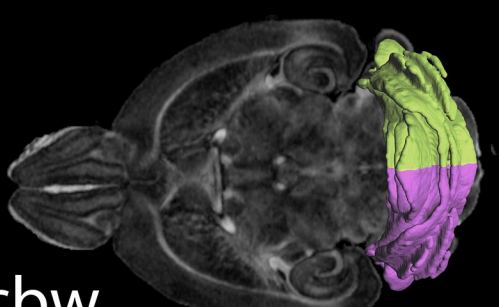
1



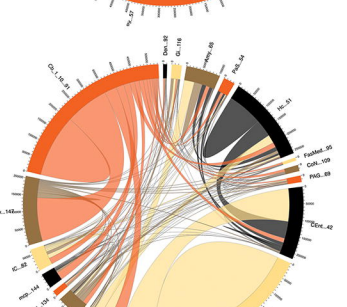
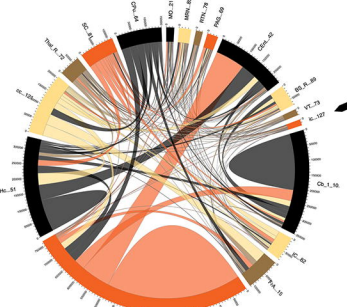
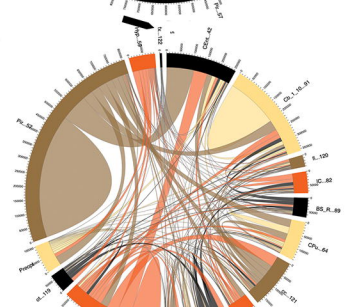
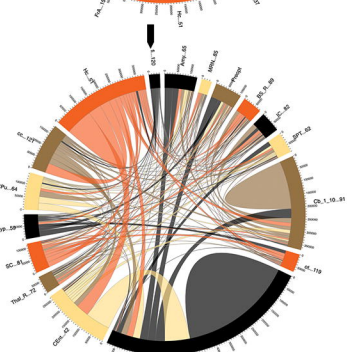
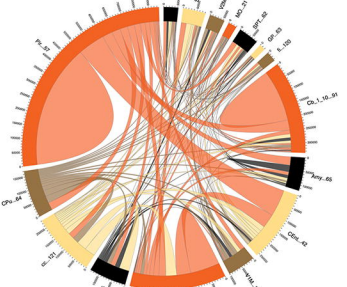
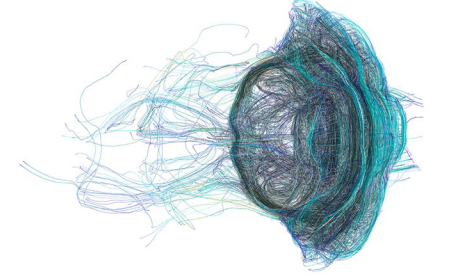
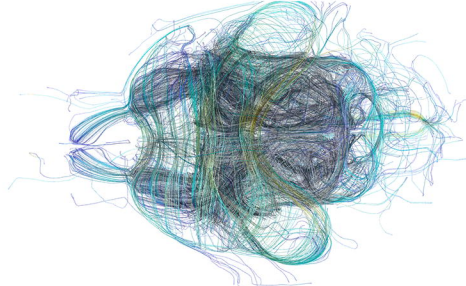
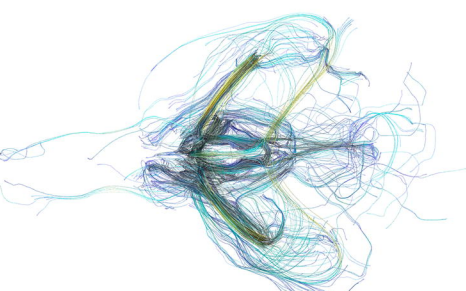
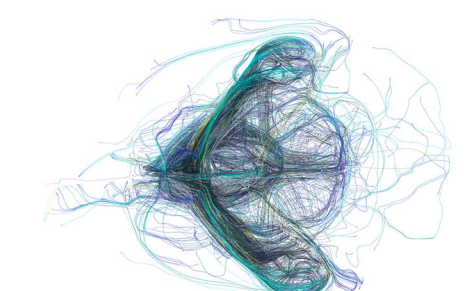
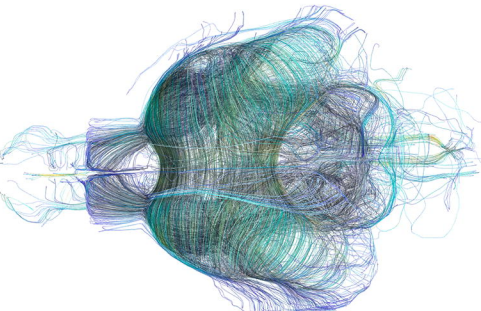
fx

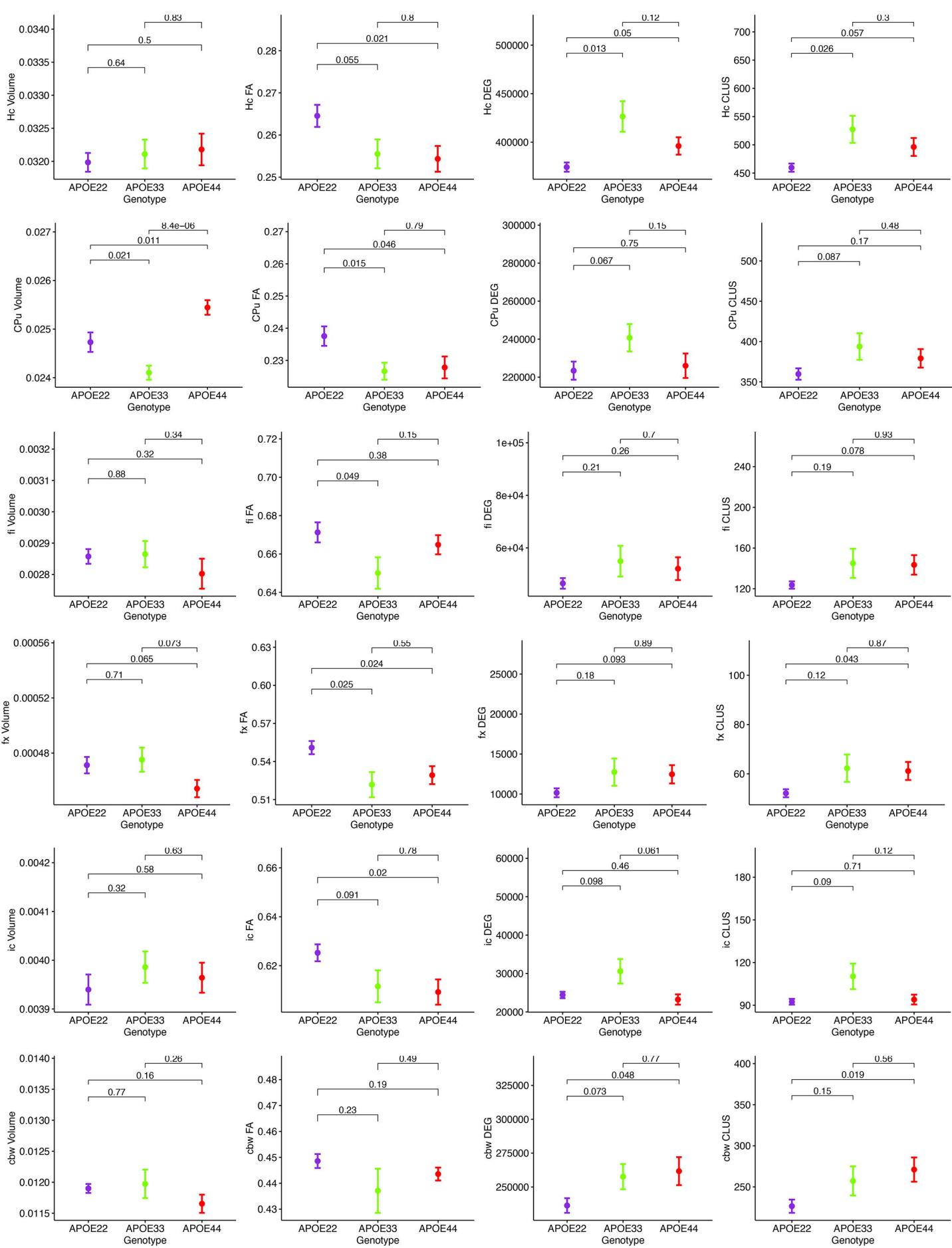


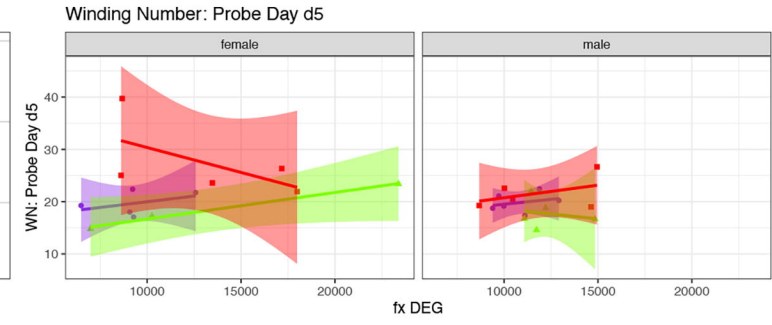
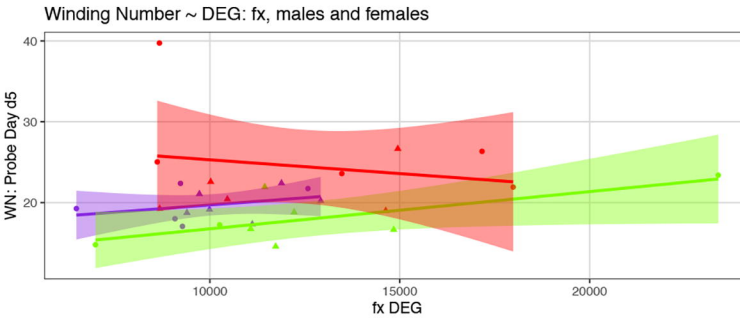
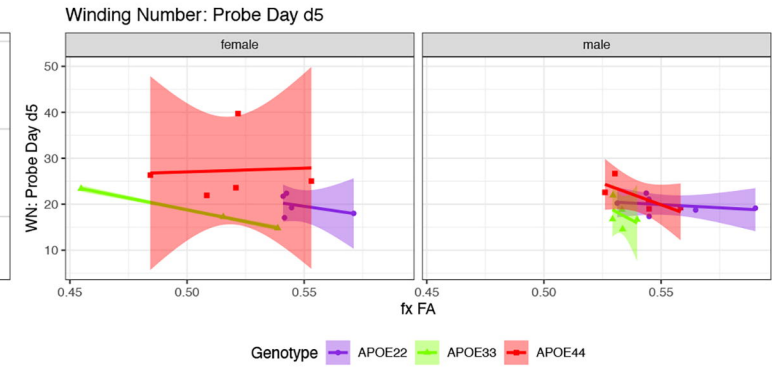
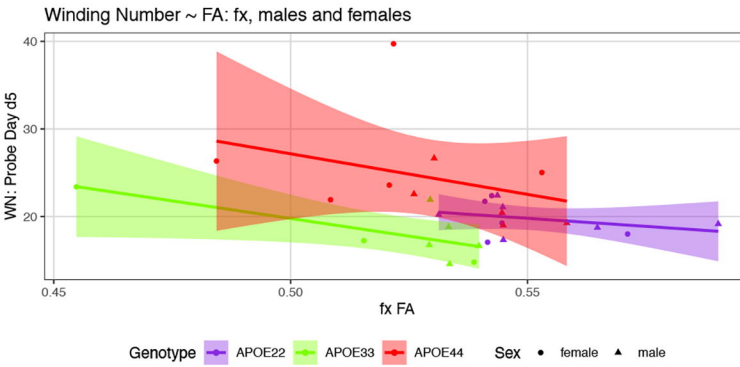
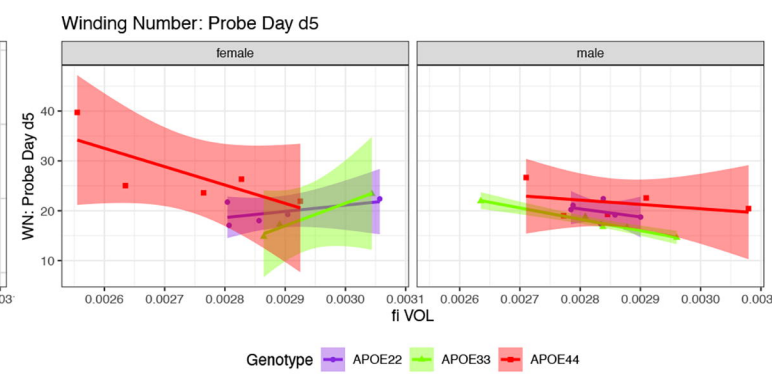
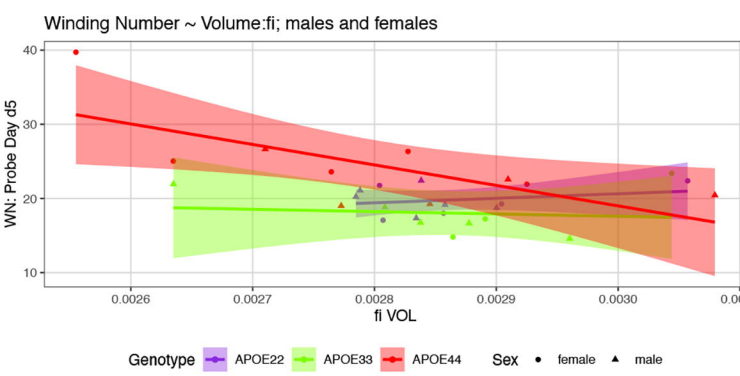
ic



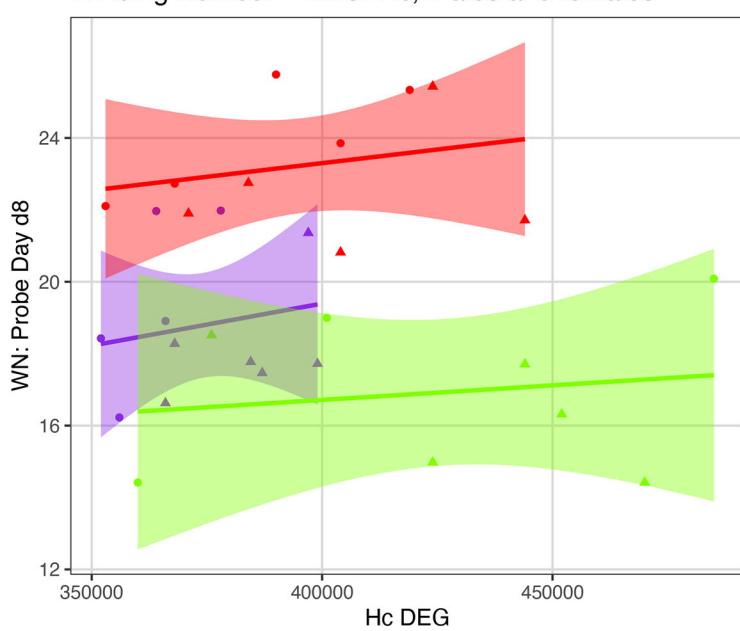
cbw





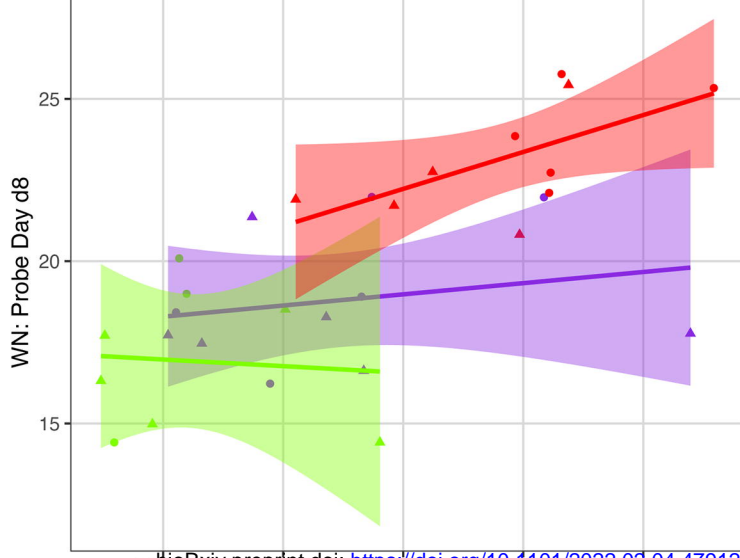


### Winding Number ~ DEG: Hc, males and females



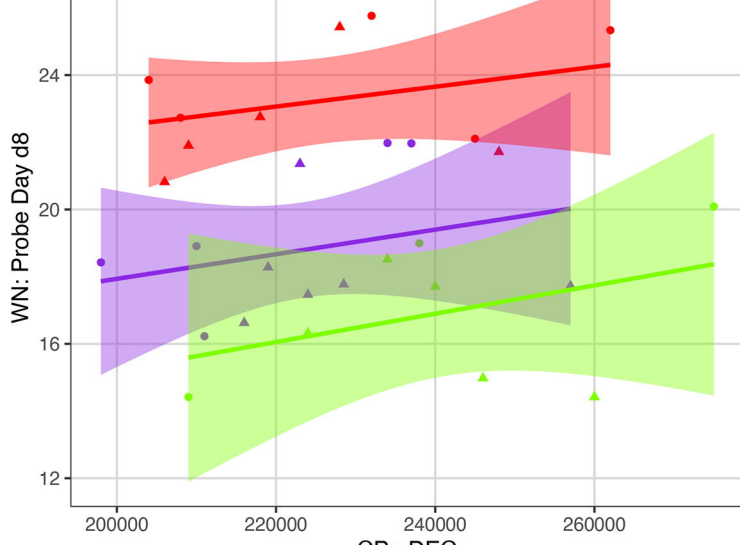
Genotype • APOE22 ▲ APOE33 ■ APOE44 Sex • female ▲ male

### Winding Number ~ Volume:CPu; males and females

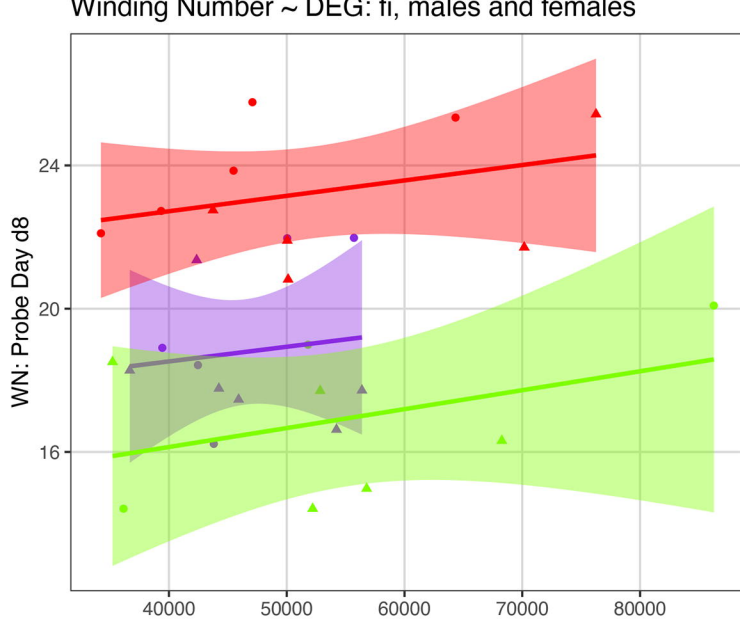


bioRxiv preprint doi: <https://doi.org/10.1101/2022.02.04.479128>; this version posted February 8, 2022. The copyright holder for this preprint (which was not certified by peer review) is the author/funder, who has granted bioRxiv a license to display the preprint in perpetuity. It is made available under aCC-BY-ND 4.0 International license.

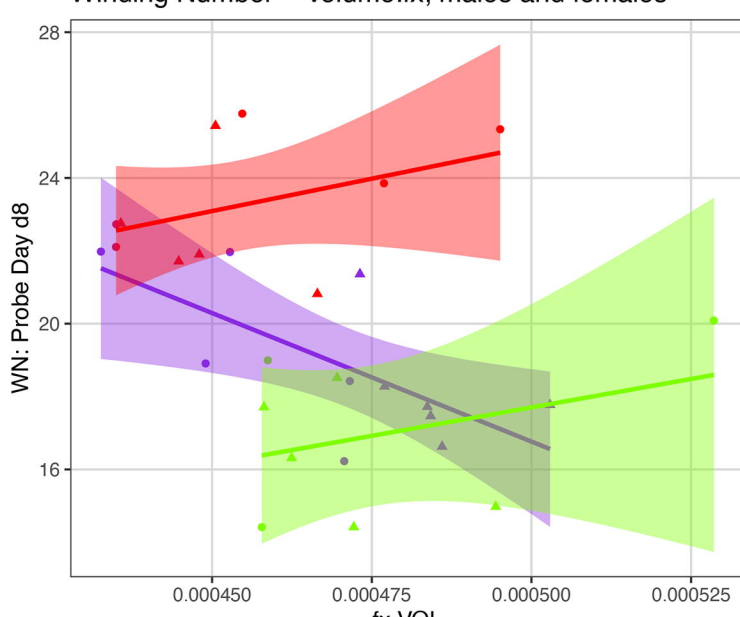
### Winding Number ~ DEG: CPu, males and females



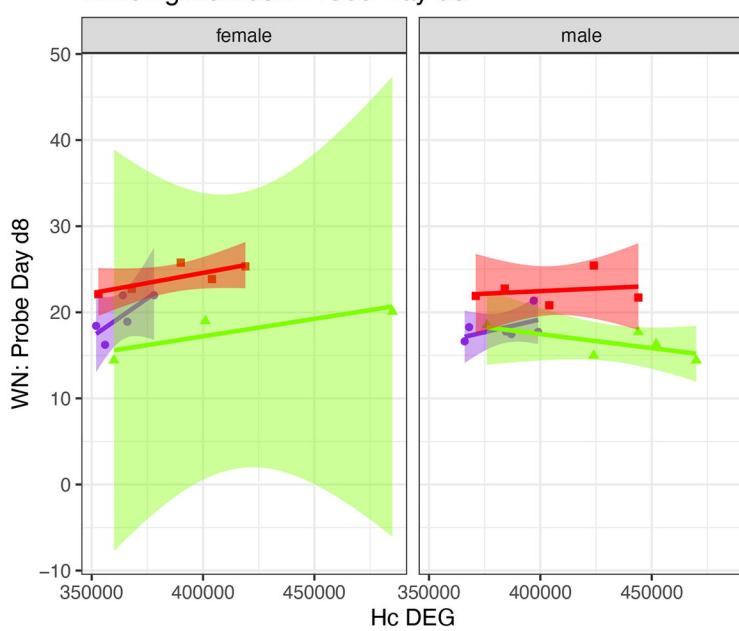
### Winding Number ~ DEG: fi, males and females



### Winding Number ~ Volume:fx; males and females

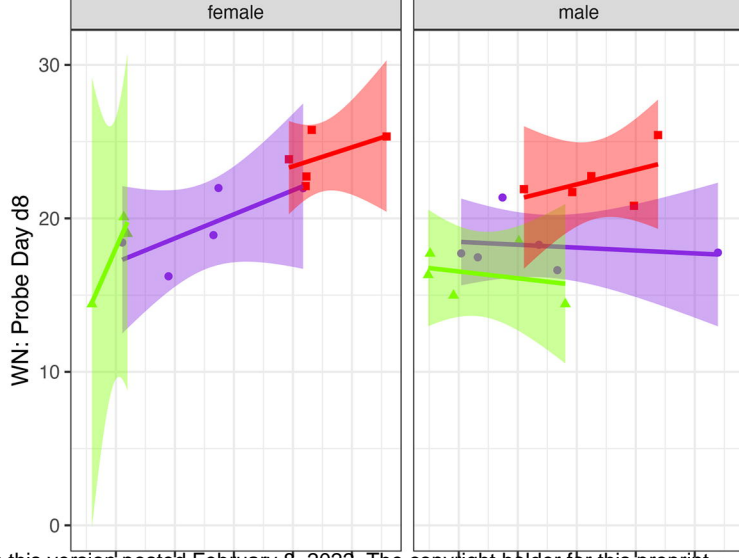


### Winding Number: Probe Day d8



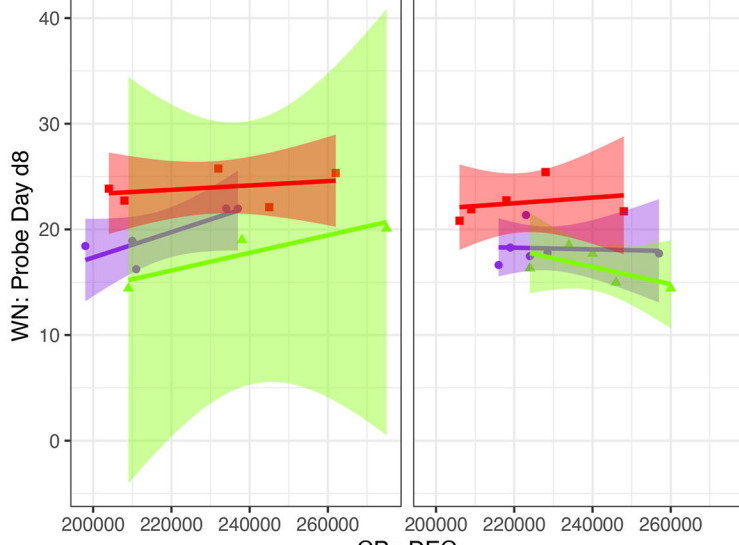
Genotype • APOE22 ▲ APOE33 ■ APOE44

### Winding Number: Probe Day d8

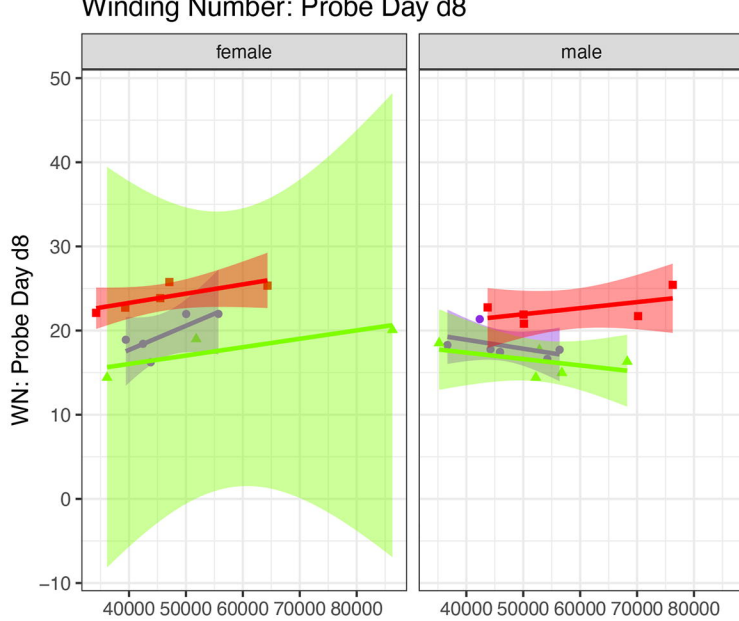


bioRxiv preprint doi: <https://doi.org/10.1101/2022.02.04.479128>; this version posted February 8, 2022. The copyright holder for this preprint (which was not certified by peer review) is the author/funder, who has granted bioRxiv a license to display the preprint in perpetuity. It is made available under aCC-BY-ND 4.0 International license.

### Winding Number: Probe Day d8



### Winding Number: Probe Day d8



### Winding Number: Probe Day d8

